CERN - EUROPEAN ORGANIZATION FOR NUCLEAR RESEARCH

Lectures held at the
Herbstschule für Hochenergiephysik
Maria Laach, Eifel, Germany
14-24 September 1976

CERN/EP/PHYS 77-40
17 August 1977

ACCELERATOR NEUTRINO PHYSICS

H. Wachsmuth

CERN, Geneva, Switzerland

HW/ef

CONTENTS

		Page
1.	ν-EPISTEMOLOGY	
1.1	Invention and discovery of the neutrino (1930-1938)	4
1.2	Universality of weak interactions (1949)	5
1.3	V-A: In weak interactions parity is not conserved (1956)	6
1.4	Weak interactions are mediated by intermediate vector-bosons (W's) (1960)	10
1.5	$\nu_\mu \neq \nu_e$ (1961)	11
1.6	Cabibbo angle (1963)	11
1.7	Quarks (1964), partons (1968) and quark-partons (1969)	12
1.8	Neutral currents (1973)	14
1.9	Charm (1974)	19
2.	ν-TECHNOLOGY	21
2.1	Principle of neutrino experiments	21
2.2	Neutrino beam	22
2.2.1	Production of ν-parents	22
2.2.2	Focusing of ν-parents	23
2.2.3	Decay of ν-parents	27
2.2.4	Shielding	28
2.2.5	Neutrino beam monitoring and spectrum determination	32
2.3	Neutrino detectors	35
2.3.1	The ideal ν-detector	35
2.3.2	Bubble chambers	36
2.3.3	Counters, spark chambers, calorimeters	39
2.3.4	Photographic emulsions	40
2.4	List of neutrino experiments 1961-1976	40
3.	ν-NUMEROLOGY (Methods and results of data analysis)	43
3.1	Charged current interactions	44
3.1.1	$\nu N \to \mu N'$	44
3.1.2	$\nu p \to \mu + \Lambda$	49
3.1.3	$\nu N \to \mu$ + hadrons	50
3.1.4	$\nu_e N \to e$ + hadrons	57

Page

3.2 Neutral current interactions 58

3.2.1 $\bar{\nu}_\mu e \to \bar{\nu}_\mu e$ 58

3.2.2 $\nu N \to \nu$ + hadrons 59

3.3 Dilepton events

3.3.1 $\nu N \to \mu\mu$ + hadrons (in counter experiments) 63

3.3.2 $\nu N \to \mu^- e^\mp$ + hadrons (in bubble chamber experiments) 66

4. CONCLUSIONS AND OUTLOOK 70

APPENDICES 71

REFERENCES 73

INTRODUCTION

The first part is a brief description of the development of the theoretical framework from the discovery of β-decay to charm. This is necessarily incomplete [1], but should show the interplay between experiment and theory to arrive at the main ideas and most popular models used in the analysis of present neutrino physics data. Some concepts, like form factors, structure functions, conserved vector current, will be treated along with cross section analyses in part 3.

The aim of the second part is to familiarize the reader with the technological aspects of accelerator neutrino experiments. It should show what the technical requirements are to obtain reasonable numbers of analysable neutrino interactions.

In the third part, the main numerical results of the recent neutrino experiments will be derived and analyzed in some detail in the context of part 1.

1. ν-EPISTEMOLOGY (from β-decay to charm)

1.1 Invention and discovery of the neutrino

On Sunday afternoon, 1 March 1896, Becquerel discovered that uranium salt had blackened a photographic plate. Many experiments - even underground - were necessary to prove that this effect was independent of external conditions and due to electron (discovered 1897) emission by nuclei ($N \rightarrow N' + e$). Neutrino physics started when Pauli [2] proposed in 1930 "a desperate remedy to save the laws of conservation of energy and statistics, which were in serious danger because of the results of three decades of experiments with the β-decay electrons". These had led to the conclusions:

(a) the electrons are emitted by nuclei, hence are in the nucleus, so e.g. the nitrogen nucleus ^{14}N would consist of 21 fermions (14 protons and 7 electrons) which is statistically impossible (the ^{14}N-band spectrum showed Bose-Einstein statistics);

(b) the electrons emitted in the (two-body) decay are not always monoenergetic which is energetically impossible.

The remedy was a fourth elementary particle, the neutrino(*) (in addition to p, e, γ) which should exist in the nucleus, have spin ½, a mass of the order of the electron mass, and be emitted during β-decay together with an electron.

Taking up this neutrino hypothesis, Fermi [3] described β-decay as the emission of an (eν)-pair by a nucleus analogous to γ emission by an excited atom in radiation theory (fig. 1).

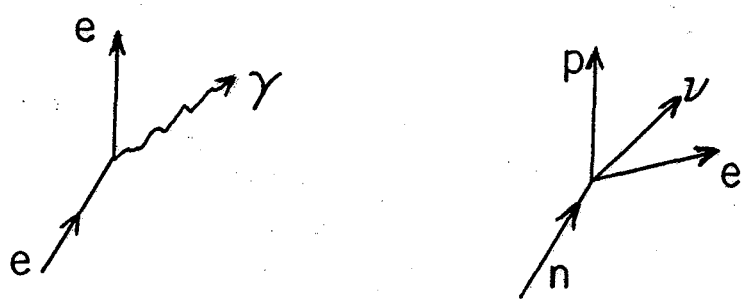

Fig. 1

(*) which Pauli called neutron, and Fermi neutrino after Chadwick's neutron discovery.

with the matrix element as we would write it today [4] for a vector current × vector current interaction

$$M = \frac{G}{\sqrt{2}} (\bar{\psi}_p \gamma_\alpha \psi_n)(\bar{\psi}_\nu \gamma_\alpha \psi_e) \tag{1}$$

where G is the Fermi coupling constant ($G = 1.4 \times 10^{-49}$ erg cm^3 or 10^{-5} m_p^{-2}).

The neutrino was detected on a cloud chamber picture in 1938 [5] by the observation of a non-collinear configuration of a β-ray and its recoil nucleus and in 1953 [6] by the observation of the inverse β-decay induced by nuclear reactor emitted antineutrinos

$$\bar{\nu} + N \rightarrow N' + e^+ . \tag{2}$$

1.2 Universality of weak interactions

Many different decay interactions like

	τ (sec)
$n \rightarrow p + e^- + \bar{\nu}$	918
${}^{14}O_8^6 \rightarrow {}^{14}N_7^7 + e^+ + \nu$	71.4
$\pi \rightarrow \mu + \nu$ (1947)	2.6×10^{-8}
$\mu \rightarrow \nu + e + \nu$	2.2×10^{-6}

and also muon capture ($\mu^- + p \rightarrow n + \nu$, capture rate $\sim 270\ Z^3$ sec^{-1}) were found to have nearly the same coupling constant, the difference in lifetime coming only from phase space:

$$\tau \sim \frac{G^2}{2} \times |M|^2 \times \text{phase space} .$$

This led to the hypothesis of the universal Fermi interaction pictured usually by an equilateral triangle [7] (fig. 2).

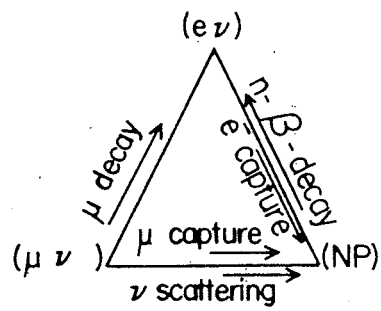

Fig. 2 Universal Fermi interactions

Each corner is called a (charged) current(*)

$$J = (e\nu),\ (\mu\nu) \text{ lepton currents, } J^L \tag{3a}$$

$$J = (NP) \qquad \text{hadron current, } J^H \tag{3b}$$

each connection line represents a current-current interaction with the matrix element (**)

$$M = \frac{G}{\sqrt{2}} \left\{ \langle J \rangle \langle J \rangle^+ + \text{herm. conj.} \right\} \tag{4}$$

The whole weak current (in 1949) is the sum of all corners

$$J = (e\nu) + (\mu\nu) + (NP)$$

and

$$M = \frac{G}{\sqrt{2}} \left\{ (e\nu)(\mu\nu) + (e\nu)(PN) + (\mu\nu)(PN) + (e\nu)(e\nu) + (PN)(PN) \right\} , \tag{5}$$

where term one describes μ-decay, term two: β-decay of the neutron $n \to p + e + \bar{\nu}$ or e capture by nuclei $e^- + p \to n + \nu$ or scattering of neutrinos off nucleons, e.g. $\bar{\nu} + p \to n + e^+$, etc. Also each corner (current) can interact with itself: $(e\nu)(e\nu)$ describes neutrino-electron scattering $\nu + e \to \nu + e$ (still unobserved, but see sect. 3.3.1) and (NP)(NP) is the weak neutron proton interaction which in principle could be detectable in certain nuclear transitions by circularly polarized photon emission [8].

1.3 V-A: In weak interactions parity is not conserved

Since particle states are described by four-component spinors, the matrix element for an interaction between four particles, like $p \to n + e + \nu$, would involve 256 coupling constants:

$$M = dr \left[\sum_{ijk\ell} g_{ijk\ell} (\psi^*_{p_i} \psi_{n_k})(\psi^*_{e_j} \psi_{\nu_\ell}) \right] \tag{6}$$

(*) Current means here just transition from initial state of a particle to its final state: $e \to \nu$, see eq. (1).

(**) $1/\sqrt{2}$ historical, to keep G at its original numerical value after parity violation discovery.

Lorentz invariance (interactions do not depend on orientation or speed of the laboratory) requires that the currents (= bilinear spinor combinations) are either

scalars ($\bar{\psi}\psi$, $\bar{\psi}\gamma_5\psi$ (pseudoscalar)) or

vectors ($\bar{\psi}\gamma_\alpha\psi$, $\bar{\psi}\gamma_\alpha\gamma_5\psi$ pseudo (axial, polar) vector) or

tensors ($\bar{\psi}\gamma_\alpha\gamma_\beta\psi$, $\bar{\psi}\gamma_\alpha\gamma_\beta\gamma_5\psi$ (pseudo tensor)),

since the products (contractions) of these give scalars, and thus reduces the 256 to 12 basic coupling constants, or rather 10 (pseudo tensor can be expressed by the other couplings): for instance for neutrino scattering $\nu + n \rightarrow \mu + p$

$$
\begin{aligned}
&(\bar{\psi}_p\ \psi_n)(\bar{\psi}_\mu\ \psi_\nu) \\
&(\bar{\psi}_p\ \gamma_5\ \psi_n)(\bar{\psi}_\mu\ \gamma_5\ \psi_\nu) \\
&(\bar{\psi}_p\ \gamma_\alpha\ \psi_n)(\bar{\psi}_\mu\ \gamma_\alpha\ \psi_\nu) \qquad \text{(Fermi's proposal eq. (1))} \qquad (7) \\
&(\bar{\psi}_p\ \gamma_\alpha\ \gamma_5\ \psi_n)(\bar{\psi}_\mu\ \gamma_\alpha\ \gamma_5\ \psi_\nu) \\
&(\psi_p\ \gamma_\alpha\ \gamma_\beta\ \gamma_5\ \psi_n)(\psi_\mu\ \gamma_\alpha\ \gamma_\beta\ \gamma_5\ \psi_\nu)
\end{aligned}
$$

or any linear combination thereof.

In 1956 Lee and Yang [9] questioned Mach's principle, i.e. that no physical process can distinguish between right-handed and left-handed coordinate systems, i.e. all physical processes conserve parity. The experimental reason for this question was the τ-θ puzzle: one and the same particle ($m_\tau = m_\theta$) decays once in 2π's (parity +1), once in 3π's (parity -1). The crucial experiment to test whether parity is violated in weak interactions was to measure the correlation between spin (axial vector) of β-active nuclei and momentum direction (vector) of the decay electrons, i.e. a pseudoscalar term (which changes sign under space reflection). The experiment [10(a)] done with polarized ^{60}Co nuclei ($\rightarrow {}^{60}\mathrm{Ni}^* + e^- + \bar{\nu}$) showed clearly parity violation: backward emission of electrons is favoured.

The idea of Lee and Yang (and Salam, Landau) was then that the lack of parity conservation was due to the neutrino spinning only in one

direction, and to describe the neutrino by 2-component spinors satisfying Weyl equations rather than by the 4-component spinors and the Dirac equation. Starting from the Dirac equation

$$\gamma_\alpha \frac{\partial\psi}{\partial x_\alpha} = - m\psi \ , \tag{8a}$$

and defining the chiral projections $\psi_\pm = \frac{1}{2}(1 \pm \gamma_5)$, one obtains

$$\gamma_\alpha \frac{\partial\psi_\pm}{\partial x_\alpha} = - m\psi_\mp \ , \tag{8b}$$

and for m = 0 and in momentum space the Weyl equation

$$\left(1 \pm \frac{\vec{\sigma} \cdot \vec{p}}{|\vec{p}|}\right) \psi_\pm = 0, \quad \frac{\vec{\sigma} \cdot \vec{p}}{|\vec{p}|} = H = \text{helicity}, \tag{8c}$$

i.e. ψ_+ describes a massless particle with negative helicity ($\vec{\sigma} \downarrow\uparrow \vec{p}$) or an antiparticle with positive helicity ($\vec{\sigma} \uparrow\uparrow \vec{p}$); and for ψ_- the correspondence is reversed. "The neutrino spinning only in one direction" means, it participates in interactions only as $\psi_+ = \frac{1}{2}(1 + \gamma_5)\psi$ or as $\psi_- = \frac{1}{2}(1 - \gamma_5)\psi$, corresponding to maximum parity violation. Charge conjugation is also violated (particle and antiparticle solutions are not symmetric) but the combined operation CP = (charge conjugation) × (spatial inversion) is well defined (CP violation - observed in K^o-decays - is not described by this theory!).

The circular photon polarization from the e capture process $^{152}Eu + e \rightarrow {}^{152}Sm^* + \nu \rightarrow {}^{152}Sm + \gamma + \nu$ [10(b)] fixed the neutrino helicity: neutrinos (all leptons) are left handed (ψ_+), antineutrinos (all antileptons) are right handed (ψ_-).

The next step was to extend this idea to all, also massive (bare) fermions. This was done first by postulating chirality invariance [11] (four fermion interaction invariant if ψ is transformed into $\psi \rightarrow \psi = \gamma_5\psi$), then by reformulating the Dirac equation as Klein-Gordon equations also for massive particles [8], then by applying mass reversal invariance [12]. So, all bare fermions are left-handed skrews

$$\psi \rightarrow \tfrac{1}{2}(1 + \gamma_5)\psi$$

and the only remaining (non gradient) coupling was

$$M = \frac{G}{\sqrt{2}} \left(\overline{\tfrac{1}{2}(1+\gamma_5)\psi_p}\ \gamma_\alpha\ \tfrac{1}{2}(1+\gamma_5)\psi_n\right)\left(\overline{\tfrac{1}{2}(1+\gamma_5)\psi_e}\ \gamma_\alpha\ \tfrac{1}{2}(1+\gamma_5)\psi_\nu\right)$$

$$= \frac{G}{\sqrt{2}} \left(\bar{\psi}_p\ (1+\gamma_5)\ \gamma_\alpha\ \psi_n\right)\left(\bar{\psi}_e(1+\gamma_5)\ \gamma_\alpha\ \psi_\nu\right), \qquad (9)$$

i.e. vector-axial vector (V-A).

This was for some time in disagreement with some experiments, especially with the electron neutrino angular correlation measured in ^{6}He, which favoured scalar-tensor coupling. But the experiments were re-done and the corrected results agreed with the V-A picture.

Now cross sections for scattering of two point like fermions via the weak interaction can be derived from eq. (9). Using the rules for Feynman graphs [4] and γ-matrix trace calculations, e.g. for $\nu + e \to \nu + e$ and $\bar{\nu} + e \to \bar{\nu} + e$ (a process not yet detected, see however sect. 1.8 and 3.3.1) one finds:

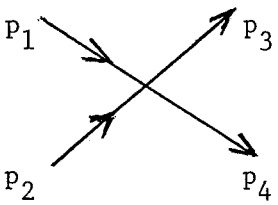

$$\frac{d\sigma}{d\cos\theta} = \frac{1}{32\pi\ s}\ |M|^2 \quad (\sqrt{s} = \text{total center of mass energy})$$

with:

	$\nu e \to \nu e$ (s-wave)	$\bar{\nu} e \to \bar{\nu} e$ (p-wave)
	ν left-handed, e left-handed	$\bar{\nu}$ right-handed, e left-handed
$\lvert M\rvert^2$	$64\ G^2(p_1p_2)(p_3p_4) = 16\ G^2s^2$	$64\ G^2(p_1p_3)(p_2p_4) = 16\ G^2u^{2*)}$
$\frac{d\sigma}{d\cos\theta}$	$\frac{G^2}{\pi}\ s$	$\frac{G^2}{\pi}\ s\ (\frac{1+\cos\theta}{2})^2$
$\frac{d\sigma}{dy}$	$\frac{G^2}{\pi}\ s$	$\frac{G^2}{\pi}\ s\ (1-y)^{2(*)}$ (10a)
σ_{total}	$\frac{G^2}{\pi}\ s = \frac{2G^2m_e}{\pi}\ E_\nu = 1.6\times 10^{-41}\ E_\nu(\text{GeV})\ \text{cm}^2$	$\frac{1}{3}\ \sigma^{\nu e\to\nu e}$ (10b)

*) $y = \frac{1-\cos\theta}{2} = \frac{p_2q}{p_1p_2} = \frac{\text{energy transfer } (E_1-E_3)}{E_1}$, $q = p_1-p_3$; $s = (p_1+p_2)^2 = 4(m^2+k^2) \approx 4k^2 \approx 2mE_1$, $u = (p_1+p_3)^2 = -2k^2\ (1+\cos\theta)$, k = c.o.m. mom. of ν.

1.4 Weak interactions are mediated by intermediate vector bosons (W's)

In order to prevent the cross section eq. (10) from becoming infinite with increasing E_ν, the exchange of a weak interaction quantum W of charge ±1 (charged current interaction, ν turns into e^-), spin 1 (weak interactions change spin), large mass (weak interactions have short range) and vector type (it has to couple 4-component currents) has been postulated [13] in complete analogy to QED:

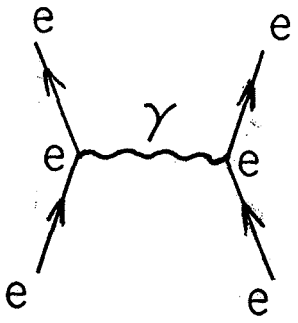

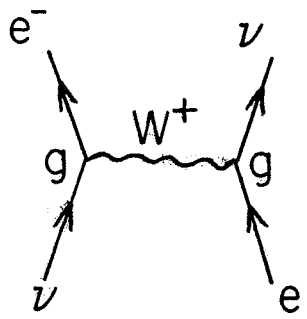

$$M = e^2 \, (\bar{e}\gamma_\alpha e) \, \frac{1}{q^2} \, (\bar{e}\gamma_\alpha e)$$

$$M = g^2 \left(\bar{e}\gamma_\alpha(1+\gamma_5)\right) \frac{\delta^{\alpha\beta} - \frac{q^\alpha q^\beta}{m_W^2}}{q^2 - m_W^2} \left(\bar{\nu}\gamma_\alpha(1+\gamma_5)e\right)$$

$$\text{with } (q^2 \to 0) \; \frac{g^2}{m_W^2} = \frac{G}{\sqrt{2}}$$

However, 2-boson exchange still leads to quadratic divergences due to the longitudinal polarization of the massive W [14], which is not the case in QED:

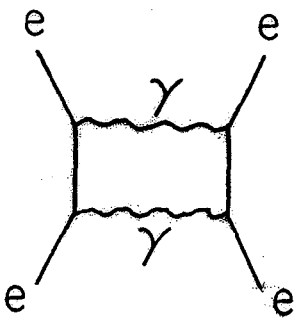

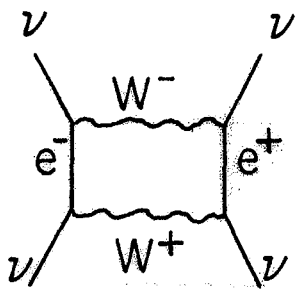

$$\delta \to \int \frac{d^4q}{q^6} \to \text{finite} \qquad \delta \to \int \frac{d^4q}{q^2} \to \text{infinite} \qquad (11)$$

In neutrino experiments the intermediate vector boson W could in principle be discovered by direct production of W's through a process similar to electromagnetic Bremsstrahlung. From the fact that no such production has been observed so far, one concludes that the W mass must be greater than 4 GeV/c^2.

1.5 $\nu_\mu \neq \nu_e$ (1962)

The most important result of the first accelerator neutrino experiment (performed at Brookhaven [15]) was the fact that a beam of neutrinos from $\pi \to \mu\nu$ decay produced only events with μ^-, and not equal numbers of events with e^- and μ^-. This proved the existence of muonic neutrinos, ν_μ (coupled to muons, e.g. in $\pi \to \mu\nu_\mu$, $K \to \pi\mu\nu_\mu$) as distinct from electronic neutrinos, ν_e (coupled to electrons, e.g. in $n \to p\, e\nu_e$, $K \to \pi e\nu_e$), described by different lepton numbers L_μ, L_e:

	e, ν_e	$e^+, \bar{\nu}_e$	$\bar{\mu}, \nu_\mu$	$\mu^+, \bar{\nu}_\mu$	hadrons
L_μ	0	0	1	-1	0
L_e	1	-1	0	0	0

which are separately conserved [16].

1.6 Cabibbo angle (1963)

From comparison of the decay rates

$$\frac{\Lambda \to Pe\nu_e}{N \to Pe\nu_e}\ ,\quad \frac{K \to \mu\nu_\mu}{\pi \to \mu\nu_\mu}\ ,\ \text{and others,}$$

it was clear that the effective coupling constants in strangeness changing ($\Delta S \neq 0$) weak interactions were $\sim \sqrt{20}$ smaller than in $\Delta S = 0$ weak interactions, thus breaking the weak interaction universality eq. (1) and (2). The universality was rescued by redefining [17] the weak hadron current eq. (3b):

$$J^H = \cos\theta_c \cdot J^{H,\Delta S=0} + \sin\theta_c \cdot J^{H,\Delta S=1}$$
$$= \left(\bar{P}\gamma_\alpha(1+\gamma_5)N\right) \cdot \cos\theta_c + \left(\bar{P}\gamma_\alpha(1+\gamma_5)\Lambda\right) \sin\theta_c \,. \tag{12}$$

The universality triangle now becomes:

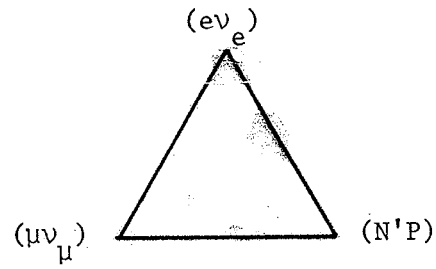

with $N' = N\cos\theta_c + \Lambda\sin\theta_c$ (θ_c = "Cabibbo angle"). The cross section ratio $\sigma^{\Delta S=1}/\sigma^{\Delta S=0} = \tan^2\theta_c = 0.056$ and the empirical selection rules

$$\Delta S = 1, \quad \Delta I = \tfrac{1}{2},$$
$$\Delta S = 0, \quad \Delta I = 1,$$

and $\Delta Q = \Delta S$, $\Delta S \leqslant 1$ have been confirmed in many decay interactions. The test of this scheme in neutrino experiments is difficult, since existing neutrino detectors (sect. 2.3) can identify strange particles only with small efficiency: $K^\pm$ are undistinguishable from $\pi^\pm$, K_L^o and the K_s^o and Λ-decays into neutrals are rarely visible. In addition, the $\Delta Q = \Delta S$ rule, which forbids e.g.

$$\nu + n \to \mu^- + \Lambda + \pi^+ \quad (Q_n - Q_{\Lambda\pi^+} = -1,\ S_n - S_{\Lambda\pi^+} = +1),$$

is expected to be apparently violated in the charm model (sect. 1.9). However, single Λ-production by antineutrinos, $\bar{\nu} + p \to \mu^+ + \Lambda$ [18], has been observed (sect. 3.1.2).

1.7 Quarks (1964), partons (1968) and quark partons

Similarities between strange and non-strange particles in strong interactions had been raised to a symmetry principle: strong interactions are invariant under strangeness change, and in the same way as isospin invariance puts hadrons into isomultiplets ((p,n), (π^+,π^o,π^-), $(\Sigma^+,\Sigma^o,\Sigma^-)$, ...), strangeness invariance puts hadrons into SU_3-multiplets (with B = baryon number, S = strangeness, I_3 = 3. Isospin component), two of which are shown in fig. 3.

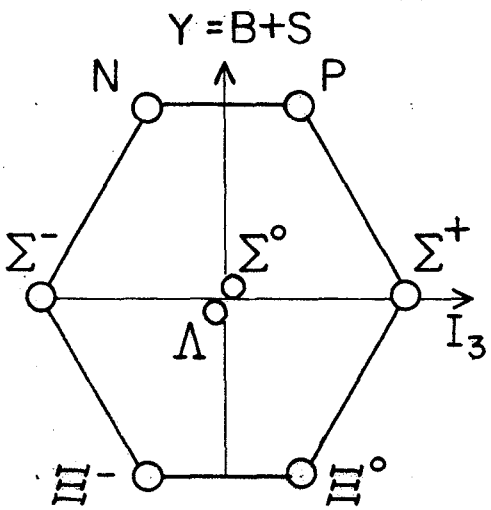

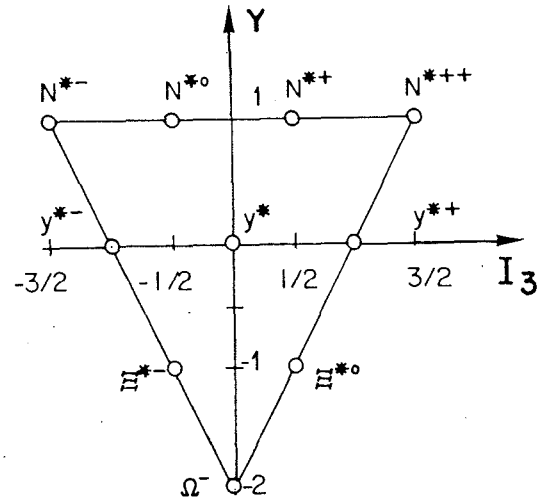

Fig. 3 SU_3 - $1/2^-$ - octet SU_3 - $3/2^+$ - decuplet

All physical particles are postulated [19] to be built from three hypothetical fundamental constituents(*) - called quarks (spin ½) - being the basic representation of the SU_3 symmetry group (fig. 4).

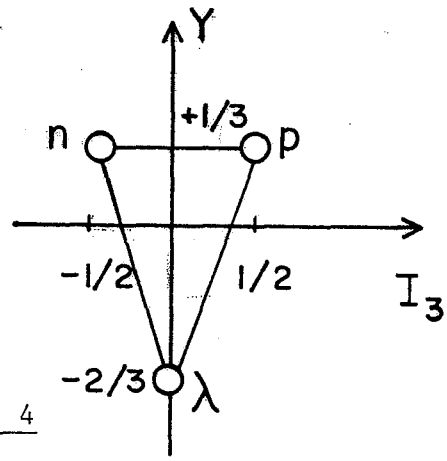

Fig. 4

A proton is then:

$$p = \begin{pmatrix} p \\ p \\ n \end{pmatrix}$$

a neutron

$$N = \begin{pmatrix} n \\ n \\ p \end{pmatrix}$$

a lambda

$$\Lambda = \begin{pmatrix} p \\ n \\ \lambda \end{pmatrix}$$

Weak interactions violate strangeness; a p-quark does not know a priori whether it should turn into an n-quark or into a λ-quark. Hence, for weak interactions we may define "Cabibbo rotated" quarks

$$n' = n \cos\theta_c + \lambda \sin\theta_c \tag{13a}$$

and, by analogy

(*) However, a 3-quark state is anti-symmetric, whereas baryon wave functions are symmetric; hence at least for spin statistics reasons, one more degree of freedom is needed [20]: each quark in three colours, and hadrons mix the colours such that they are colour singlets.

$$\lambda' = -n \sin\theta_c + \lambda\cos\theta_c, \tag{13b}$$

but λ' does not seem to participate in weak interactions. All weak interactions (fig. 5), seem to happen really between 4 leptons and 3 quarks, for example, Λ-production by $\bar{\nu}_\mu$ - P-scattering might be pictured as in fig. 6:

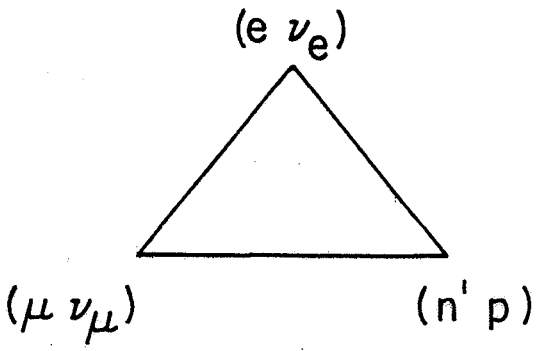

Fig. 5

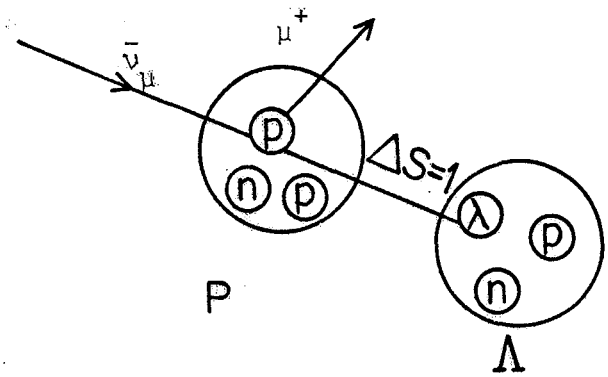

Fig. 6

When it became evident in 1968 that electrons [21] and neutrinos [22] scatter off nucleons - in high energy and momentum transfer collisions - as if the nucleon was made of points - partons [21] - namely by the large cross section for high momentum transfers(*), the idea suggested itself that these partons are the above quarks (quark-parton model). Then, total neutrino cross sections should just be the sum of neutrino quark cross sections and hence have the same behaviour as νe scattering cross sections eq. (10a,b). That this is nearly so, will be seen in sect. 3.1.3.

1.8 Neutral currents (discovery 1973)

The electromagnetic current is a neutral current, the electromagnetic interaction being due to (neutral) photon exchange

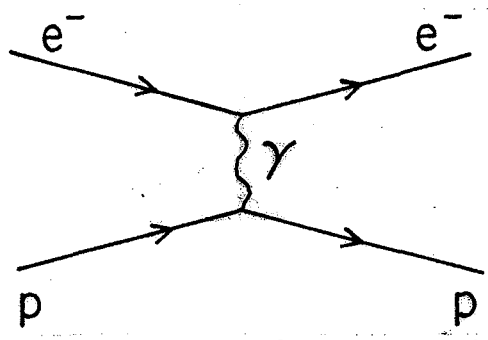

(*) A situation similar to Rutherford's α-scattering experiments showing that atoms have hard nuclei.

The weak current was, prior to 1973, supposed to be charged, the weak interaction being due to (charged) W exchange:

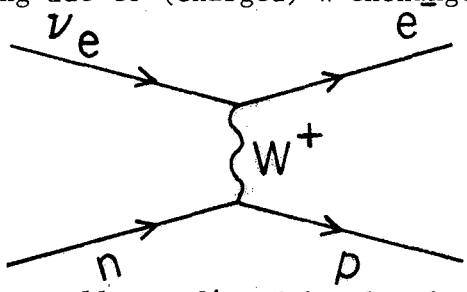

This was experimentally confirmed by the absence ($< 10^{-6}$) of neutral current interactions like $K \to \pi\mu\mu$, $\to \pi\nu\nu$, and others.

In 1973, however, on the Gargamelle(*) neutrino film tracks of single electrons were discovered which could not be interpreted other than by muonic $\bar{\nu}$ scattering off atomic electrons [23]

$$\bar{\nu}_\mu + e^- \to \bar{\nu}_\mu + e^-$$

which can only happen through a weak neutral current interaction:

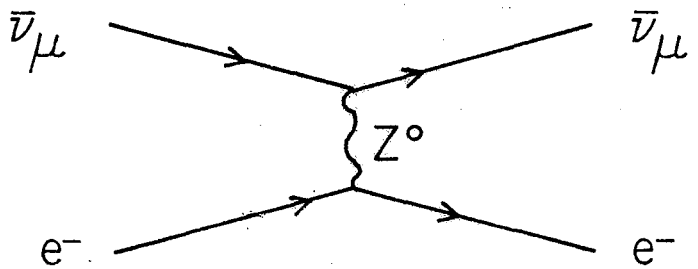

assumed to happen via the exchange of a neutral massive vector-boson Z^o.

On the same film [24] and also in counter experiments [25] neutrino interactions were discovered which had only hadrons in the final state and which could - with high probability - only be interpreted as due to muonic neutrinos scattering off nucleons without turning into muons (sect. 3.2.3)

$$\nu_\mu + N \to \nu_\mu + \text{hadrons},$$

i.e. by a neutral current interaction

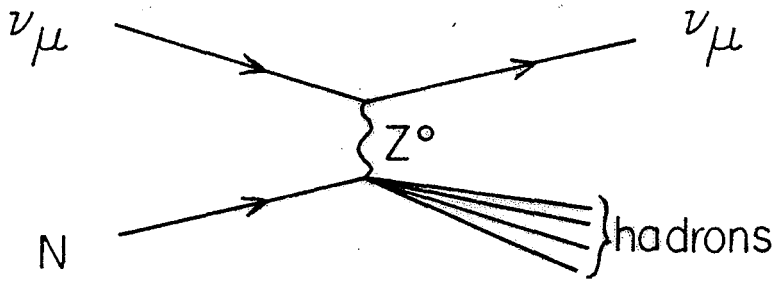

(*) Heavy liquid bubble chamber, see sect. 2.3.2.

The Z^o allowed two things highly desired by theorists:

(a) renormalization of the weak interaction theory, i.e. overcoming the difficulty of infinite cross sections eq. (11) and simultaneously

(b) unification of electromagnetic and weak interactions.

There is extensive [26] and didactic [27] literature showing this in detail. Here, only the main steps will be enumerated.

The non-renormalizability of weak interaction theory comes from the longitudinal polarization of the massive W. The renormalizability of the electromagnetic theory (QED) is due to gauge invariance (cf. table I (A)).

TABLE I

Local gauge invariance

A	B
Electromagnetic field	Yang-Mills field
Lagrangian of a free fermion field $L_o = \bar{\psi}(x)\ (i\not{\partial} - m)\psi(x)$ is invariant if $\psi(x) \to e^{ie\alpha}\ \psi(x)$ which is a phase transformation, same rotation everywhere in space. $\longrightarrow$ Lorentz invariance ($\to$ charge conservation)	$\psi(x) \to e^{\frac{1}{2}ig(\vec{\tau}\ .\ \vec{\beta})}\ \psi(x)$ (τ = Pauli matrix), which is isospin rotation, same everywhere in space. $\longrightarrow$ Isospin invariance
If rotation different in every space point (fixed locally): $\psi(x) \to e^{ie\alpha(x)}\ \psi(x)$ then L still invariant, if $\partial_\mu \to D_\mu = \partial_\mu - ieA_\mu$ (covariant derivative, A_μ is <u>massless</u> gauge field) and $A_\mu \to A_\mu + \partial_\mu\ \alpha(x)$	If rotation different in every space point: $\psi(x) \to e^{\frac{1}{2}ig(\vec{\tau}\ .\ \vec{\beta}(x))}\ \psi(x)$, then L still invariant, if $\partial_\mu \to D_\mu = \partial_\mu - \frac{1}{2}ig\ \vec{\tau}\ .\ \vec{\beta}_\mu$ and if the isospin carrying B field is transformed like $\vec{B}_\mu \to \vec{B}_\mu + g(\vec{B}_\mu \times \vec{\beta}) + \partial_\mu\ \vec{\beta}(x)$

Yang and Mills have (already in 1954) shown that by introducing isospin multiplets of vector-bosons local gauge invariance can be generalized to isospin rotation (table I (B)). However, invariance requires, as in the photon case, massless bosons, and one fact which is certainly known

about the intermediate vector bosons is that they are heavy ($m > 4$ GeV/c^2, from the short range, even pointlike behaviour, of the weak interactions). The next step is then to generate masses by the Higgs-mechanism (1964) of spontaneous gauge symmetry breaking. How this is done is outlined in Appendix A, following closely the lectures of Iliopoulos. In order to demonstrate the concept of spontaneous symmetry breaking the phenomenon of ferromagnetism is often used as an example (e.g. S. Weinberg, Sci. Am. July 1974):

"... The equations governing the electrons and iron nuclei in a bar of iron obey rotational symmetry, so that the free energy of the bar is the same whether one end is made the north pole by magnetization or the south. At high temperatures the curve of energy versus magnetization has a simple *U* shape that has the same rotational symmetry as the underlying equations [*see illustration below*]. The equilibrium state, the state of lowest energy at the bottom of the *U*, is also a state of zero magnetization, which shares this symmetry. On the other hand, when the temperature is lowered, the lowest point on the *U*-shaped curve humps upward so that the curve resembles a *W* with rounded corners. The curve still has the same rotational symmetry as the underlying equations, but now the equilibrium state has a definite nonzero magnetization, which can be either north or south but which in either case no longer exhibits the rotational symmetry of the equations. We say in such cases that the symmetry is spontaneously broken. A tiny physicist living inside the magnet might not even know that the equations of the system have an underlying rotational symmetry, although we, with our superior perspective, find this easy to recognize. Reasoning by analogy, we see that a symmetry principle might thus be exactly true in a fundamental sense and yet not be visible at all in a table of elementary-particle masses. . . ."

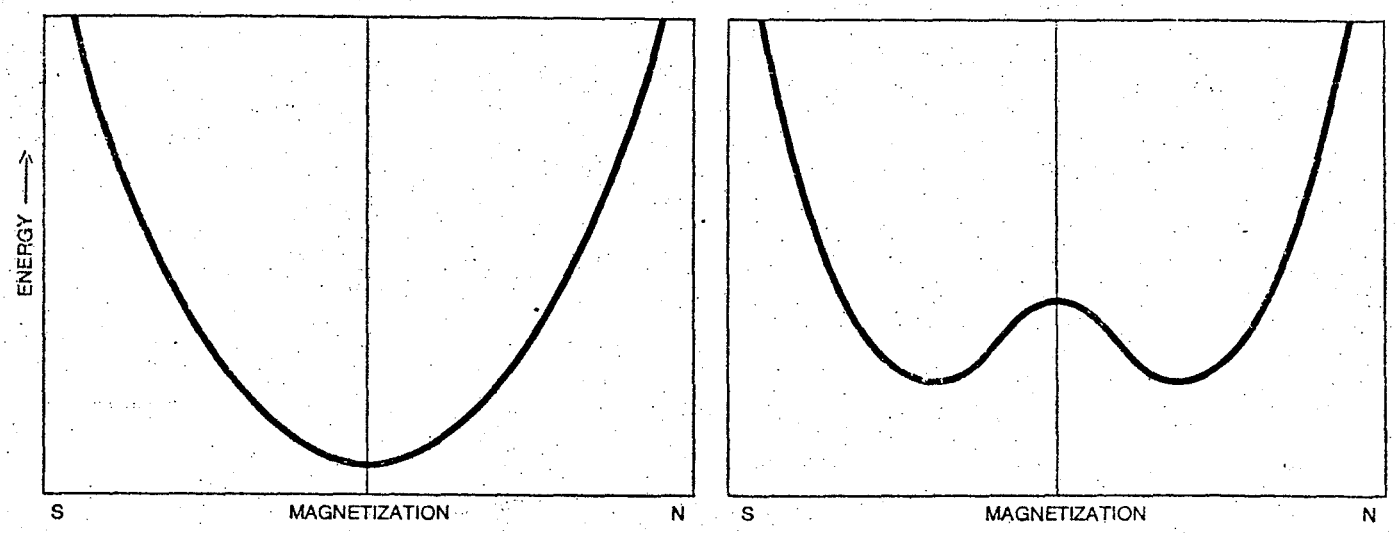

EXAMPLE OF "BROKEN" SYMMETRY can be found in the two different curves that result when one plots the free energy v. magnetization for a bar magnet at high temperature (*left*) or at low temperature (*right*). The magnet naturally seeks a state of minimum free energy. At high temperature this is a state of zero magnetization, a state that exhibits perfect symmetry between north and south. At low temperature the equilibrium state shifts to one of nonzero magnetization, which can be either north or south, even though the free-energy curve is still perfectly symmetrical between north and south. In this case physicists say that the symmetry is spontaneously broken. The author invokes a similar breaking of symmetry to unify the electromagnetic and weak interactions.

Weinberg (and independently Salam) suggested [28] such a broken symmetry group which contains the unbroken gauge symmetry group of electromagnetism with the massless photon and - as the photon's relatives - the massive charged ($W^{\pm}$) and neutral (Z^{o}) vector bosons associated with broken symmetries. And in 1971 t'Hooft [29] demonstrated that this theory is renormalizable.

This model consists of (with A_μ = photon field, $Z_\mu = Z^o$ field)

1 doublet of left-handed leptons $\frac{1}{2}(1+\gamma_5)\begin{pmatrix}\nu_e\\ e^-\end{pmatrix} = : \psi_L$

1 singlet of a right-handed lepton $\frac{1}{2}(1-\gamma_5)\, e = : \psi_R$

1 isospin triplet $\vec{W} = \left\{W^+_\mu,\ W^-_\mu,\ Z_\mu \cos\theta + A_\mu \sin\theta\right\}$

1 isospin singlet $B_\mu = \left\{ -Z_\mu \sin\theta + A_\mu \cos\theta\right\}$

with the following interaction between leptons and vector bosons:

$$L = \bar{\psi}_L \gamma_\mu (g \cdot \vec{\tau} \cdot \vec{W}_\mu - g' B_\mu)\psi_L - g'' \bar{\psi}_R \gamma_\mu \psi_R B_\mu . \qquad (14)$$

From the condition that the electromagnetic interaction for electrons

$$(\bar{e}_L \gamma_\mu e_L) A_\mu (-g \sin\theta - g'\cos\theta) - (\bar{e}_R \gamma_\mu e_R) A_\mu g'' \cos\theta$$

must be equal to $e(\bar{e}_L \gamma_\mu e_L + \bar{e}_R \gamma_\mu e_R)A_\mu$,

follows: $g \sin\theta + g' \cos\theta = g'' \cos\theta = -e$.

From the condition that the neutrino makes (in 1. order) no electromagnetic interactions

$$g \sin\theta - g' \cos\theta = 0$$

follows: $g'/g = \tan\theta$

and hence $e = -2g \sin\theta = -\dfrac{2gg'}{\sqrt{g^2 + g'^2}}$. (15)

The Weinberg angle θ is the only free parameter in this model and can be determined from the observed rate of $\bar{\nu}_\mu e$ scattering (sect. 3.2.1) and after extension of the model to hadrons (implying further assumptions) also from $\nu_\mu + N \to \nu_\mu$ + hadrons (sect. 3.2.2).

1.9 Charm (1974)

Now we have weak neutral currents (and a nice model describing them), so in addition to the charged hadron currents eq. (3b) $J^{+} = (\bar{p}n')$, $J^{-} = (n'\bar{p})$ with $W^{\pm}$ exchange, we also have

$$J^{oH} = (pp) - (n'n')$$

with Z^{o} exchange; however, the current

$$(n'n') = (nn) + (\lambda\lambda) + (n\lambda) + (\lambda n)^{(*)}$$

contains also transitions between neutron and λ-quarks (eq. (13a)) which are strangeness changing ($\Delta S = 1$) neutral ($\Delta Q = 0$) currents, and these do not exist in nature (cf. page 15). The way out of this dilemna is the introduction of a fourth quark, c, called charmed quark [30] and to complete the universality triangle to a square (fig. 7) in which also the somewhat lost λ'-quark eq. (13b) finds its place. In this model the production of charmed particles by neutrinos is predicted which would be observable by the leptonic and/or hadronic decay of these particles into strange particles ($\Delta C = \Delta S$).

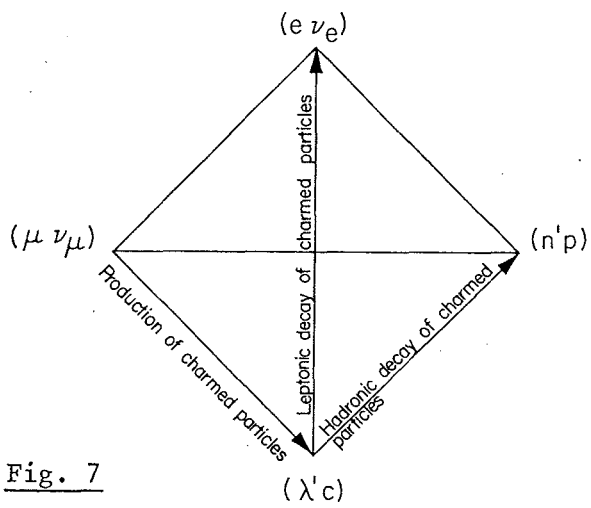

Fig. 7

Now, the neutral current has still the terms (pp), (n'n'), but in addition (cc) and ($\lambda'\lambda'$)

(*) $J^{+} = (\bar{p}n')$ is short for the isospin raising current (see eq. (12))

$$J^{+}_{a} = \bar{p}\,\gamma_\alpha\,(1+\gamma_5)n\,\cos\theta_c + \bar{p}\,\gamma_\alpha\,(1+\gamma_5)\lambda\,\sin\theta_c$$

and

$$J^{o}_{\alpha} = \bar{p}\,\gamma_\alpha\,(1+\gamma_5)p - \cos^2\theta_c\,\bar{n}\,\gamma_\alpha\,(1+\gamma_5)n - \sin^2\theta_c\,\lambda\,\gamma_\alpha\,(1+\gamma_5)\lambda$$
$$- \sin\theta_c\,\cos\theta_c\left(\bar{n}\,\gamma_\alpha\,(1+\gamma_5)\lambda + \bar{\lambda}\,\gamma_\alpha\,(1+\gamma_5)n\right).$$

$$
\begin{aligned}
J^{o} &= (pp) + (cc) - (n'n') - (\lambda'\lambda') \\
&\qquad\qquad\qquad\qquad\qquad\qquad\quad (nn) + (\lambda\lambda) - (n\lambda) - (\lambda n) \\
&\qquad\qquad\qquad\qquad (nn) + (\lambda\lambda) + (n\lambda) + (\lambda n) \\
&= (pp) + (cc) + 2(nn) + 2(\lambda\lambda)
\end{aligned}
\tag{16}
$$

with the effect that the strangeness changing transitions $(n\lambda)$ cancel (because of the minus sign in λ', see eq. (13b)).

As we know, in 1974 in a Brookhaven experiment studying $p + Be \rightarrow e^{+} + e^{-}$ + anything and in a SLAC experiment studying $e^{+} + e^{-} \rightarrow e^{+} + e^{-}$ + anything, peaks were discovered (Koch and Krammer lectures of this School) interpreted as $(c\bar{c})$ states (J/ψ), and in 1976 at SLAC and DESY $K^{-}\pi^{+}\pi^{+}$ and $K^{-}\pi^{+}$ peaks were interpreted as the charmed mesons D^{+} and D^{o}. Also in 1974, the FNAL neutrino experiment reported di-muon events (sect. 3.3.1) interpreted as the production and subsequent leptonic decay of charmed particles

$$
\begin{aligned}
&\nu + N \rightarrow \mu^{-} + C + \ldots \\
&\qquad\qquad\qquad\quad \hookrightarrow \mu^{+} + \nu + \ldots
\end{aligned}
$$

and bubble chamber neutrino experiments observed interactions (sect. 3.3.2) compatible with the same scheme but the charmed particle decaying into $e^{+} + \nu + \ldots$.

The four quarks have the following quantum numbers for charge, baryon number, isospin, strangeness and charm - all quarks appearing in three colours (cf. footnote p. 13) -

	Q	B	I	S	C
c	2/3	1/3	0	0	1
p	2/3	1/3	1/2	0	0
n	-1/3	1/3	1/2	0	0
λ	-1/3	1/3	0	-1	0

and the production of a charmed baryon by neutrinos might be pictured as shown in fig. 8.

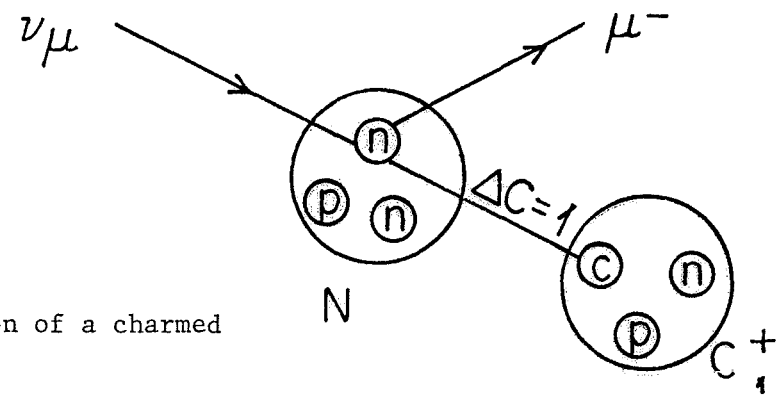

Fig. 8

Production of a charmed baryon.

with the subsequent decay (immediately, $\tau < 10^{-12}$ sec) of the charmed particle into a strange particle ($\Delta C = \Delta S$) and ($\ell\ \nu_e$) or hadrons.

In Appendix B a list of possible charmed particles is given, copied from ref. [31].

2. ν-TECHNOLOGY

2.1 Principle of neutrino experiments

Because of the small neutrino cross section $\sigma^{\nu} \approx 3\sigma^{\bar{\nu}} \approx 10^{-38}$ E(GeV) cm^2 (page 9 and sect. 2.3.2) neutrino beams of high intensity and neutrino detectors of large mass are necessary to obtain reasonable event rates. For instance, in a detector of 1 ton ($N_N = 6 \times 10^{29}$ nucleons) traversed per accelerator pulse by 10^{10} neutrinos ($\sim 10^6$ ν's/cm^2) of 1 GeV energy

$$N_{ev} = \sigma \cdot N_{\nu} \cdot N_N = 10^{-38} \cdot 10^6 \cdot 6 \cdot 10^{29} = .006 \text{ events},$$

i.e. every 170 pulses, a neutrino interaction would occur.

The source of neutrinos in accelerator neutrino beams is the weak decay of pions and kaons ($\pi \to \mu + \nu_\mu$, $K \to \mu + \nu_\mu$, $\pi + \mu(e) + \nu_\mu(\nu_e)$) produced by protons in external targets (sect. 2.2.1) and focused by magnetic fields (sect. 2.2.2). The neutrinos are separated from the other particles produced in the target, from the parents which have not decayed and from the muons by means of several 1000 t of absorber material (shielding, sect. 2.2.4). The neutrino interactions are observed in large bubble chambers (sect. 2.3.2), counter arrangements and spark chambers (sect. 2.3.3),

or in nuclear emulsions (sect. 2.3.4), depending on the aim of the experiment. In addition, neutrino experiments require a good knowledge of the neutrino spectrum (absolute intensity as a function of energy) since the incident neutrino is unobservable.

In so called wide-band neutrino beams, essentially all parents produced in the target are used requiring special focusing devices with large momentum and angle acceptance (magnetic horn) and yielding neutrino spectra from lowest (several 100 MeV) to highest energy (close to proton energy). In so-called narrow-band "dichromatic" neutrino beams the parents are momentum selected ($\Delta p/p \sim 5\%$) by quadrupole lenses yielding a neutrino spectrum of two peaks, one from pions, the other one from kaons, as will become clear in sect. 2.2.3.

A schematical layout of neutrino experiments is shown in fig. 9.

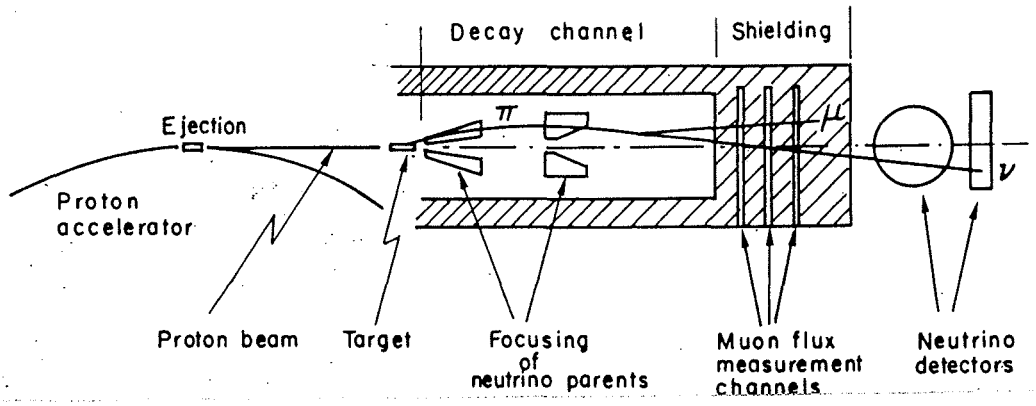

Fig. 9 Principle of neutrino experiments.

2.2 Neutrino beams

2.2.1 Production of neutrino parents

Pions and kaons are produced - along with other particles - in proton nucleus collisions in external targets onto which the ejected proton beam is focused, with nearly exponential distribution in momentum and angle.

Extensive measurements were done at 24 GeV proton energy [32] (and will have to be done at 400 GeV) in order to determine this distribution as accurately as possible.

In order to obtain maximum particle output, target shape and material must be optimized. It must be two to three proton absorption lengths long and its diameter must be fitted to the proton beam shape (accounting for multiple scattering of the protons), in order to keep π and K reabsorption small. Intra-nuclear absorption can be reduced by using material with small nuclei. In the CERN wide-band neutrino experiments 90 to 130 cm long boron carbide (B_4C) and beryllium targets of 3-8 mm diameter were used.

2.2.2 Focusing of ν-parents

(a) Wide-band beams

Mesons are produced with a mean transverse momentum of about $p_t \approx 0.3$ GeV/c. Hence the natural divergence of a beam of 4-15 GeV pions (from 26 GeV protons) is 75 to 20 mrad and the parent beam width after about 100 m (length necessary for decay and shielding) is 2-8 m; in addition, the neutrino intensity is further reduced by the decay angle distribution. Since neutrino detectors - for practical reasons - cannot be much bigger than 1 or 2 m in radius, it is necessary to focus the particles produced in the target. This is achieved with rotationally symmetric magnetic fields [33],"magnetic horns", (principle shown in fig. 10) the

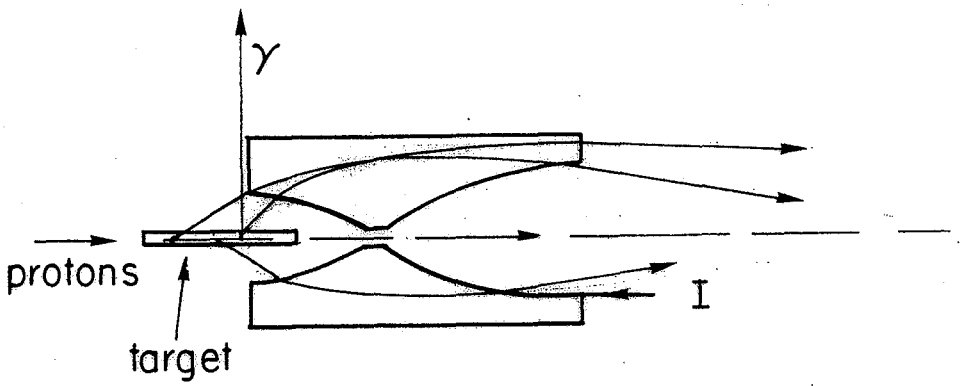

Fig. 10 Principle of magnetic horn

inner conductor of which can be shaped such that most of the production angles and momenta over the entire target length are accepted and bent towards the detector. Focusing efficiency is increased by using a second (and sometimes a third) lens of this type [34].

Since transverse momenta up to $\sim$ 800 MeV/c must be focused, and

$$B\ell = 0.033\ p_t, \text{ (B in kG, } \ell \text{ in m, } p_t = \text{ in MeV/c)},$$

$$B = 0.2\ I/r, \text{ (I in kA, r in cm)},$$

currents of several 100 kA are required. Hence these devices must be pulsed (fig. 11) and mechanically strong (pressure between end plates $= 6.3\ (I/d)^2 \sim 13\ t/m^2$). Figs 12(a) and (b) show one of the CERN magnetic horns.

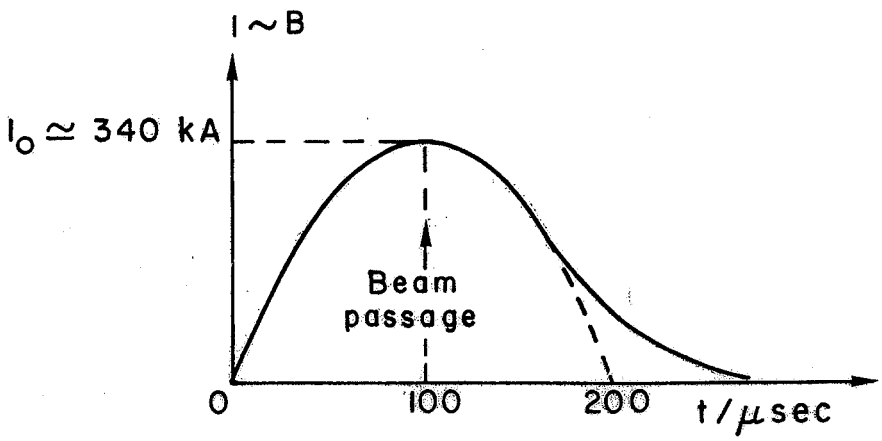

Fig. 11 Typical horn current form

(b) Narrow-band beams

In principle, magnetic horns can also be shaped such that they focus only a small momentum band, but a cleaner selection and better adjustable angular divergence is achieved by using quadrupole beams. If the ejected proton beam is not pointing towards the detector (fig. 13) - as in the present narrow-band beam at the CERN SPS, wide-band beam background flux from parents decaying before the momentum selection is further reduced.

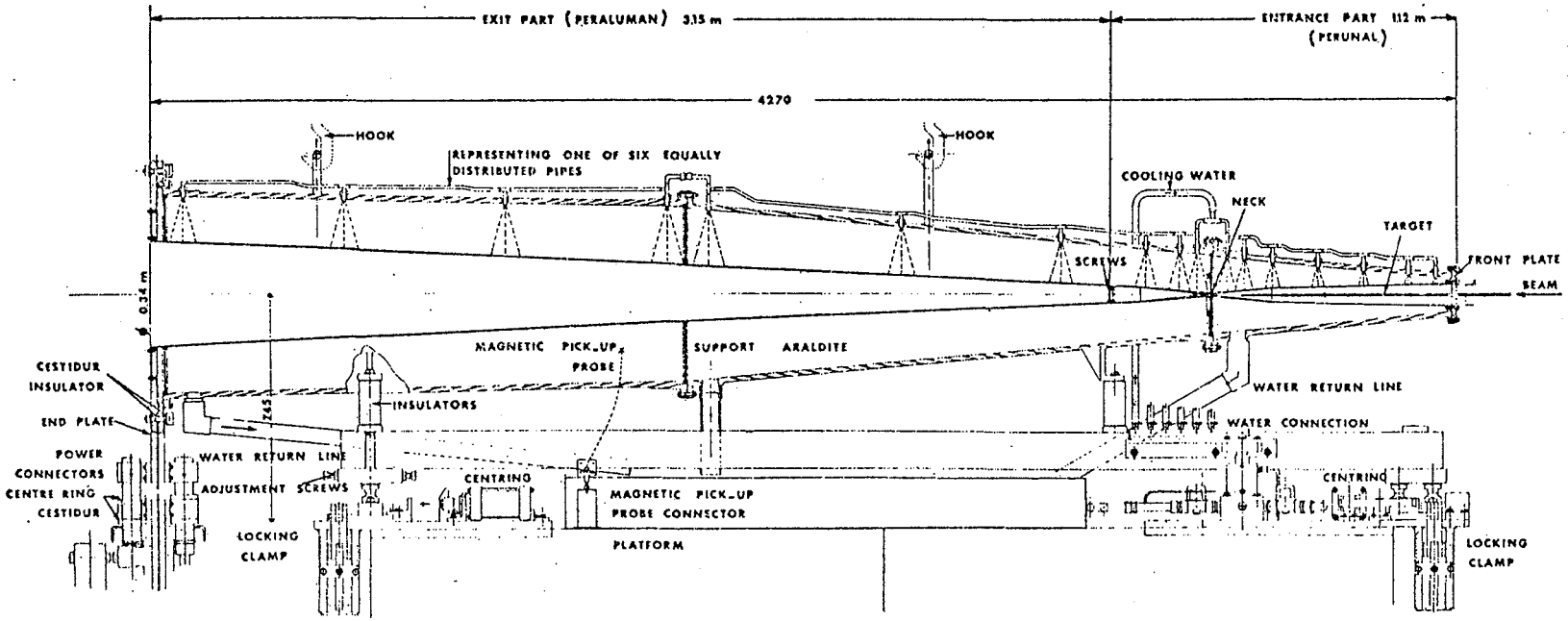

Fig. 12(a) Magnetic horn

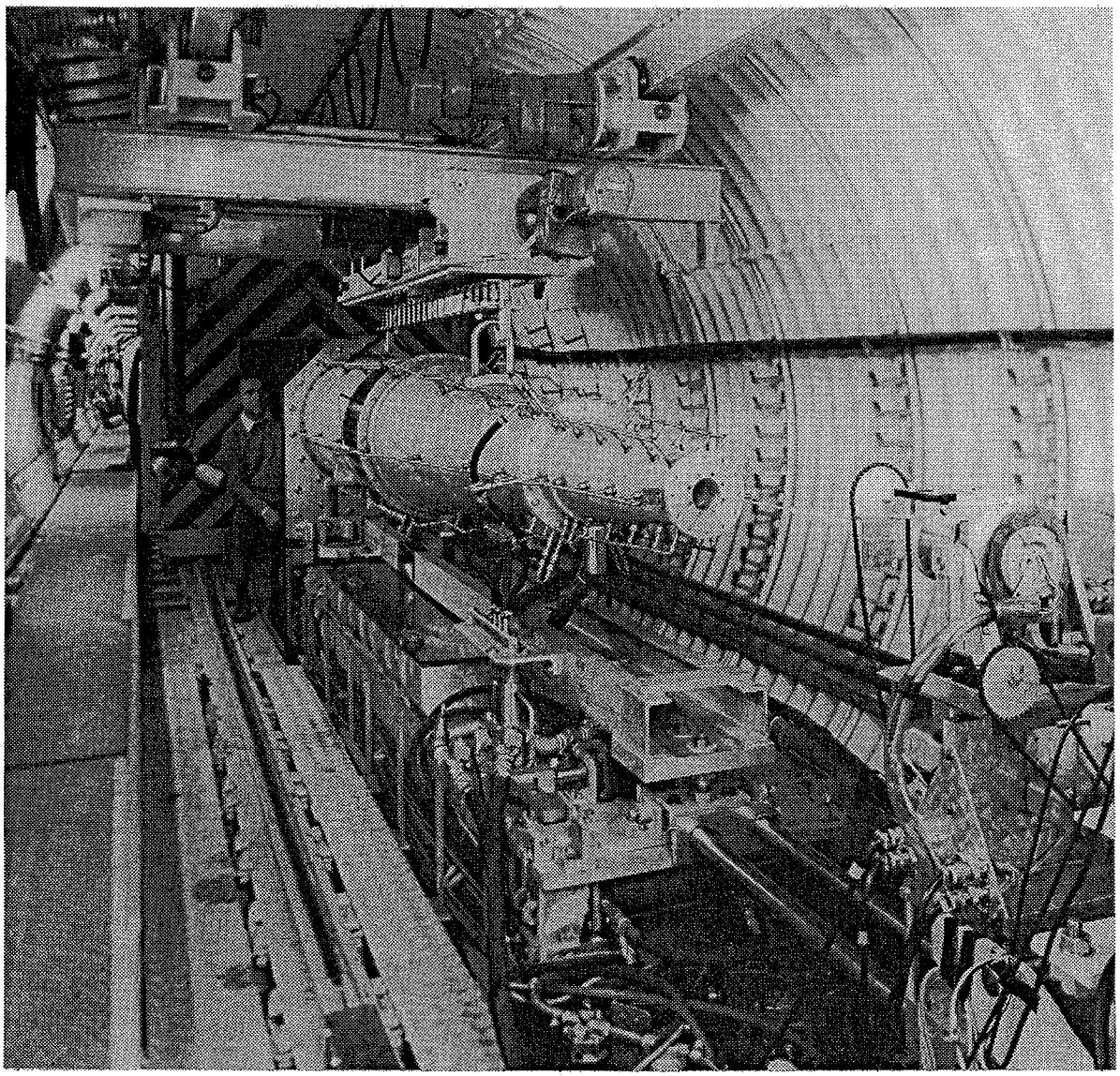

Fig. 12(b) Horn in neutrino tunnel, target and its mounting on the righthand side.

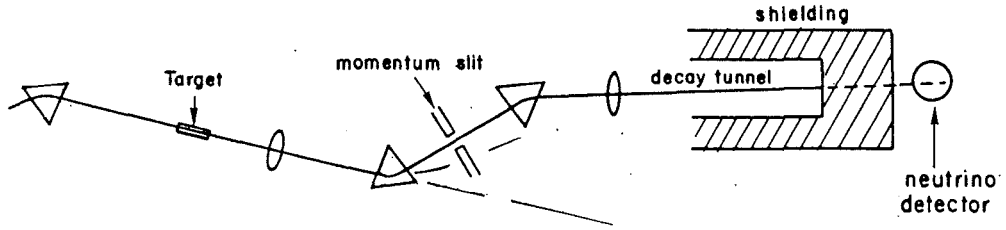

Fig. 13 Principle of narrow-band neutrino beam

2.2.3 Decay of ν-parents and ν-spectra

The exponential drop of neutrino spectra with energy is caused by the energy distribution of the parents of the target. The "fine structure" of neutrino spectra is given by the decay kinematics (fig. 14) and the relative abundance of parents and their decay branching ratios. Pions have a Q-value of 29 MeV and populate the lower energy region, kaons (Q-value 239 MeV) the higher energy region (whereas muons from both decays have energies up to the parent energy)

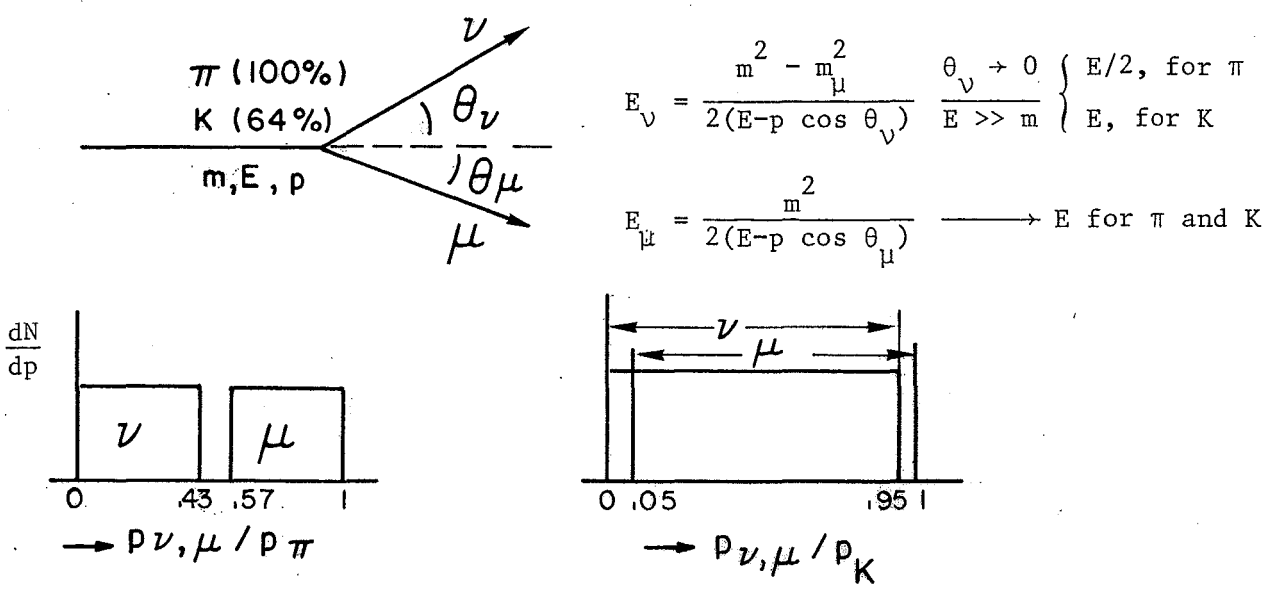

Fig. 14 Two-body decay kinematics of π and K

The three-body decay of the kaon, $K^{\pm}_{e3}$, is the high-energy source of electronic neutrinos in the neutrino beam, whereas the decay of muons from π (and K) decay, $\mu^{\pm} \rightarrow e^{\pm} \overset{(-)}{\nu}_e \overset{(-)}{\nu}_\mu$, contributes the low energy electronic neutrinos. The neutrino spectra due to these decays are calculated, using the measured centre of mass energy (E^*) distribution for electrons

$$\frac{dN_e}{dE^*} \sim \frac{(E^*_{max} - E^*)^2 \, E^{*2}}{1 - 2\,E^*/m_K} \, , \quad E^*_{max} = \frac{m_K^2 - m_{\pi^o}^2}{2\,m_K} \, , \text{ for } K_{\ell 3} \text{ decay}$$

$$\frac{dN_e}{dE^*} \sim (3m_\mu^2 - 4m_\mu \, E^*) \, E^{*2} \, , \text{ for } \mu\text{-decay}$$

as the neutrino energy distribution and transforming it - properly weighted with the parent momentum distribution - into the laboratory system.

The composition of all components in wide-band ν and $\bar{\nu}$-beams is shown in table II. Resulting neutrino spectra for experiments at three proton accelerators (Argonne National Laboratory, CERN and FNAL) are represented in fig. 15.

From fig. 14, follows that the neutrino spectrum from momentum (and sign) selected parent beams (sect. 2.2.2 (b)) of energy E, consists of two peaks, one close to E (from $K_{\mu 2}$-decay, the other close to E/2 (from $\pi_{\mu 2}$ decay), for neutrinos which traverse the detector around the beam axis ($\theta_\nu \approx 0$). Further away from the axis the two peaks shift towards lower energy (θ_ν finite). Their width depends on $\Delta p/p$ and angular divergence of the parent beam.

2.2.4 Neutrino shielding

In order to shield the neutrino detector from all particles other than neutrinos, large amounts of absorber material must be placed between the end of the decay region and the detector. Hadrons (protons not absorbed in the target, pions, kaons not decayed, and other hadrons produced in the target) are absorbed sufficiently in 15-20 absorption lengths (e.g. 2-3 m steel). The ranges of the muons - being attenuated mainly by ionization loss (δ-ray and pair production contribute only above $\sim$ 100 GeV)

TABLE II

Composition of wideband ν beam

	Positive particles focused				Negative particles focused			
	Parent	%(*)	Decay	Branch. ratio	Parent	%(*)	Decay	
Focused	π^+	∿ 80	$\mu^+ + \nu_\mu$	100	π^-	∿ 83	$\mu^- + \bar{\nu}_\mu$	"Good sign" neutrinos (except ν_μ from μ decay)
	K^+	∿ 12	$\mu^+ + \nu_\mu$	63.6	K^-	∿ 4	$\mu^- + \bar{\nu}_\mu$	
			$\pi^o + \mu^+ + \nu_\mu$	3.2			$\pi^o + \mu^- + \bar{\nu}_\mu$	
			$\pi^o + e^+ + \nu_e$	4.8			$\pi^o + e^- + \bar{\nu}_e$	
	μ^+	∿ 10	$e^+ + \bar{\nu}_\mu + \nu_e$	100	μ^-	∿ 10	$e^- + \mu_\nu + \bar{\nu}_e$	
Unfocused	K^o	∿ 3	$\pi^- + e^+ + \nu_e$	39.0	$\bar{K}^o$	∿ 7	$\pi^+ + e^- + \bar{\nu}_e$	
			$\pi^- + \mu^+ + \nu_\mu$	27.1			$\pi^+ + \mu^- + \bar{\nu}_\mu$	
	$\bar{K}^o$	∿ 3	$\pi^+ + \mu^- + \bar{\nu}_\mu$		K^o	∿ 7	$\pi^- + \mu^+ + \bar{\nu}_\mu$	"Wrong sign" neutrinos (except ν_μ from μ decay)
			$\pi^+ + e^- + \bar{\nu}_e$				$\pi^- + e^+ + \nu_e$	
Defocused	π^-		$\mu^- + \bar{\nu}_\mu$		π^+		$\mu^+ + \nu_\mu$	
	K^-		$\mu^- + \bar{\nu}_\mu$		K^+		$\mu^+ + \nu_\mu$	
			$\pi^o + \mu^- + \bar{\nu}_\mu$				$\pi^o + \mu^+ + \nu_\mu$	
			$\pi^o + e^- + \bar{\nu}_e$				$\pi^o + e^+ + \nu_e$	
	μ^-		$e^- + \nu_\mu + \bar{\nu}_e$		μ^+		$e^+ + \bar{\nu}_\mu + \nu_e$	

(*) Varying with energy.

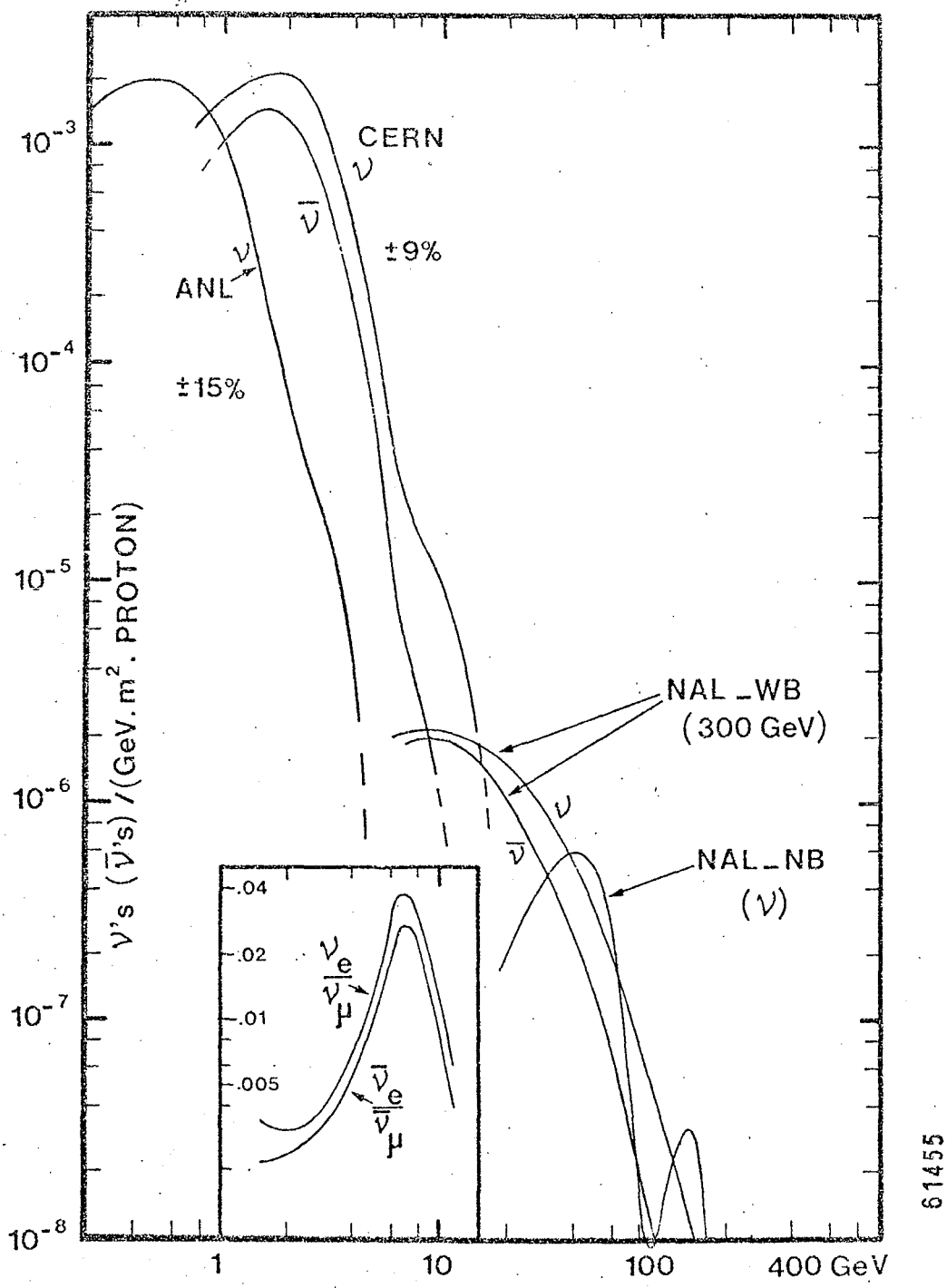

Fig. 15 Examples of neutrino spectra from three accelerators. The insert shows the fraction of ν_e spectra for the 26 GeV CERN Neutrino Beam.

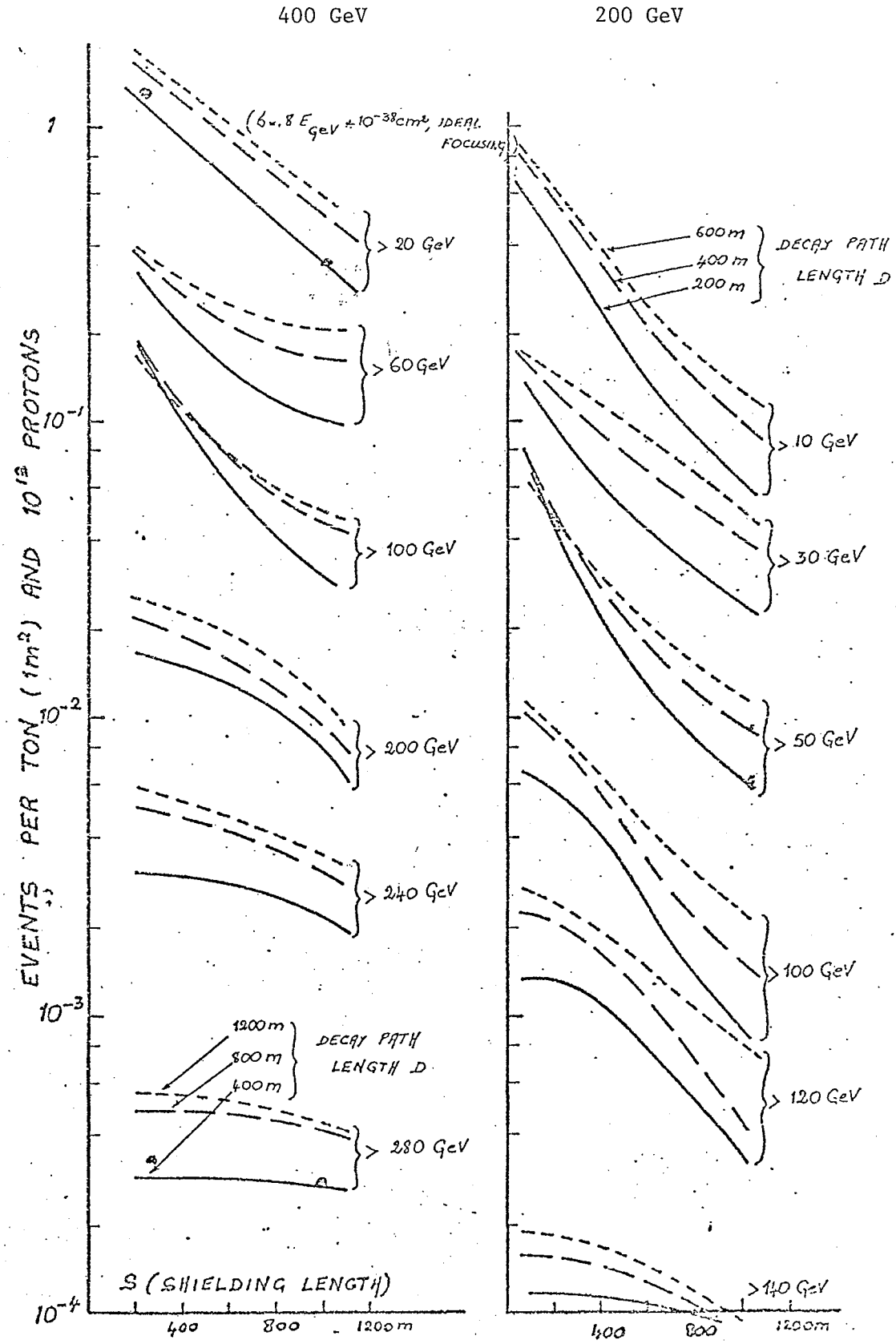

Fig. 16 Total neutrino event rates above various neutrino energies as a functions of decay and shielding length.

- determine the thickness of the shielding in beam direction, e.g. in steel about 0.7 m/GeV to which 10-15% have to be added to account for straggling (= fluctuations in energy loss).

Because of the finite divergence of neutrino beams it is necessary to use high density material ($dE/dx \sim \rho$), in order to maximise the neutrino flux intensity at the detector. This is illustrated in fig. 16, where total event rates above various neutrino energies (assuming the ν cross section to rise linearly with energy) are plotted as a function of shielding thickness for three different decay lengths.

The shielding width transverse to the beam direction is dictated by multiple scattering: multiply scattered muons must not escape by the side and back scatter into the neutrino detector. By keeping the decay tunnel diameter small (e.g. 1.2 m at the CERN SPS) - just big enough not to lose parent particles - and lining it with heavy shielding material, (steel), many muons are absorbed in the decay tunnel wall and the main shield need not be wider than 2 to 2.5 times the decay tunnel diameter.

2.2.5 Neutrino beam monitoring and spectrum determination

For neutrino experiments it is important to maximize the flux and to know its quantity and energy spectrum. Both require continuous monitoring of the beam. The proton beam intensity is usually monitored by so called beam current transformers (fig. 17).

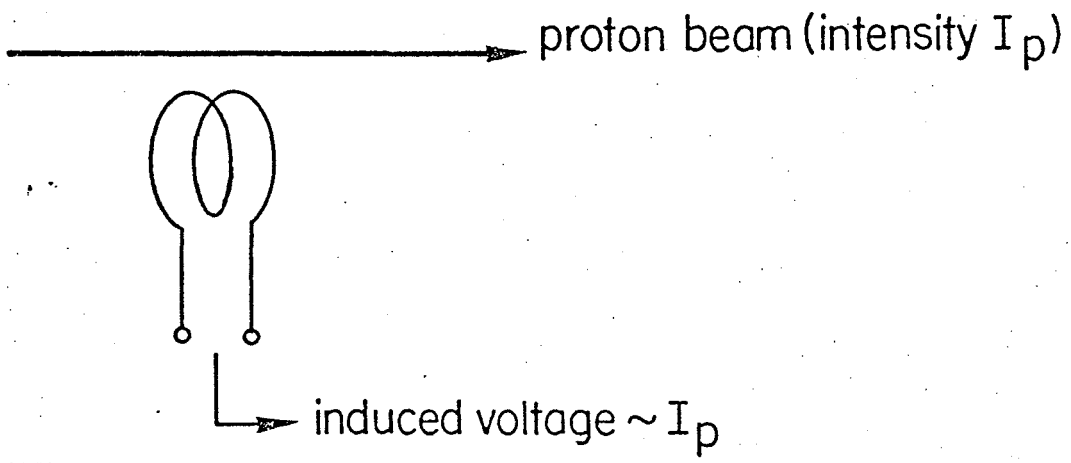

Fig. 17 Principle of beam current transformer.

The proton beam position at the target can be monitored by the signals from secondary emission of split foils (or from thermocouples) arranged symmetrically to the target.

Knowing the π and K-production by protons and the focusing properties of the parent beam, one can then predict in principle the neutrino spectrum in the detector plane. However, experimental factors like unobserved deficiencies in the focusing system, mismatch between proton beam and target, nuclear cascade effects in the target, π and K absorption and production in the decay tunnel make these predictions uncertain.

A more direct way to obtain the absolute neutrino spectrum is to measure continuously, throughout the whole neutrino experiment, the flux of muons produced along with the neutrinos by the focused π and K parents [35]. These muon fluxes are measured in the shielding - after the hadrons have been absorbed - using ionization detectors (gas ionization chambers or surface barrier solid state detectors) in several depths and radii. The muon flux relative to the incident proton beam monitors the real target efficiency, its spatial distribution monitor beam symmetry, its distribution in depth yields via the momentum range relation, the neutrino energy spectrum and its quantity measures the absolute neutrino spectrum. However, due to the Q-values of π and K decay (fig. 14), about 90% of the measurable muons come from π-decay only, and precise information on the K/π production ratio is necessary to obtain the high energy part of the neutrino spectrum (above $\sim$ 20% of the proton beam energy) which is entirely due to ν_K (fig. 14). In fig. 18 the distribution of such muon fluxes measured and calculated is shown. The calculated muon flux distribution is then fitted to the measured muon fluxes by varying the input pion spectrum (keeping the K/π ratio constant). The best estimate for the neutrino spectrum is obtained from the modified π and K spectra which make the best fit between measured and calculated muon fluxes.

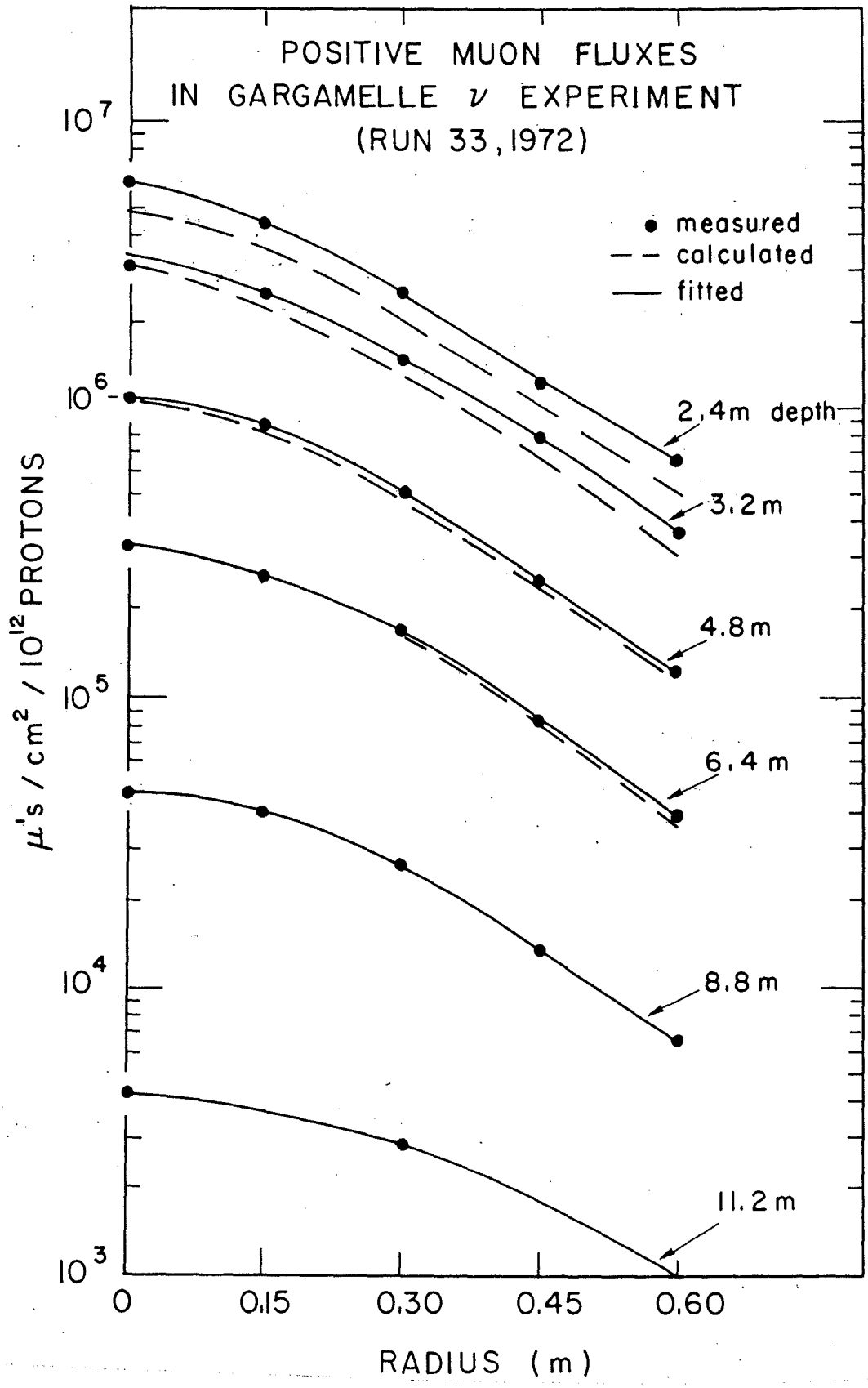

Fig. 18 Muon fluxes in the steel shield of the CERN - 26 GeV - neutrino experiment as function of depth and radius. The calculation assumes particle production in a thin target. The fit accounts for thick target effects and other inefficiencies.

2.3 Neutrino detectors

2.3.1 The ideal neutrino detector

A neutrino detector should fulfill the following requirements:

(a) Large mass because of the small ν cross section, especially for rare processes.

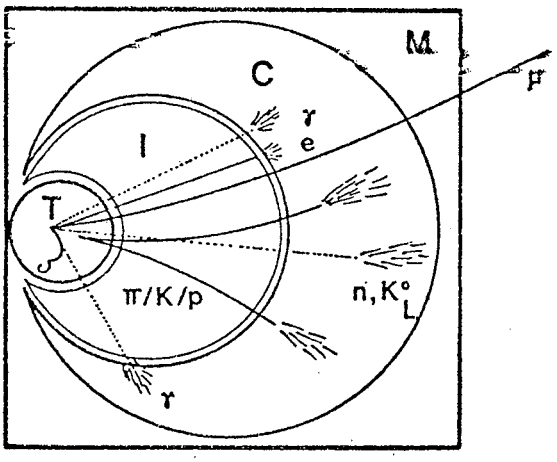

Fig. 19 T: $D_2(H_2)$ Bubble chamber
for event production
vertex observation
detection of Λ, K^o_s, $\Sigma^{\pm}$, and spectator nucleon in D_2
measurement of low momentum large angle secondaries.

I: Charged hadron identifier
for $\pi^{\pm}/K^{\pm}/p$ separation.

C: Total absorption calorimeter
for detecting and measuring gammas, neutrons and K^o_L
identifying and measuring electrons
identifying muons.

M: Magnetic field
for identifying and measuring K^o_s, Λ, low momentum electrons and hadrons in T
measuring hadron momenta in T and I
measuring muon momentum in T, I and C.

(b) Free nucleons (H_2) in order to avoid nuclear effects (secondary interaction of neutrino produced particles, binding energy, unknown state of motion of target nucleon due to Fermi momentum).

(c) Complete reconstruction of event since the incident neutrino energy and direction are unknown (even in narrow-band beams); this requires good vertex visibility (detection of Λ, K_s^o decay vertices, and to decide whether particles produced were primary or secondary) and detection, identification and measurement of all particles produced in the event.

Since no single detector technique fulfills all these requirements, such a detector would have to be a separate function hybrid system [36] according to the scheme shown in fig. 19.

2.3.2 Bubble chambers in magnetic fields (table III) [37]

They represent the closest approach to meet above requirements (b) and (c). Large hydrogen (and deuterium) bubble chambers have free (quasi-free) nucleons and good measurability (particle momentum determination from track curvature) but in general cannot distinguish between fast e, μ, π, K, have small γ and n detection probability and relatively small mass (max. 1 t). Possible extensions (partial hybridisation) are:

(i) External Muon Identification (EMI) by e.g. large area multi-wire proportional chambers placed at the downstream end of the bubble chamber after sufficient absorption material to absorb hadrons by strong interactions (fig. 20(a)).

(ii) Track Sensitive Target technique (TST) [38], essentially a H_2 (or D_2) bubble chamber inside a neon bubble chamber (fig. 20(b)), where the neon (due to the short radiation length (table III(b)) allows electron identification, some gamma detection and (due to the larger density) some neutron detection.

Heavy liquid bubble chambers (freon, neon, propane) have larger event rates (proportional to density), good electron identification,

(a)

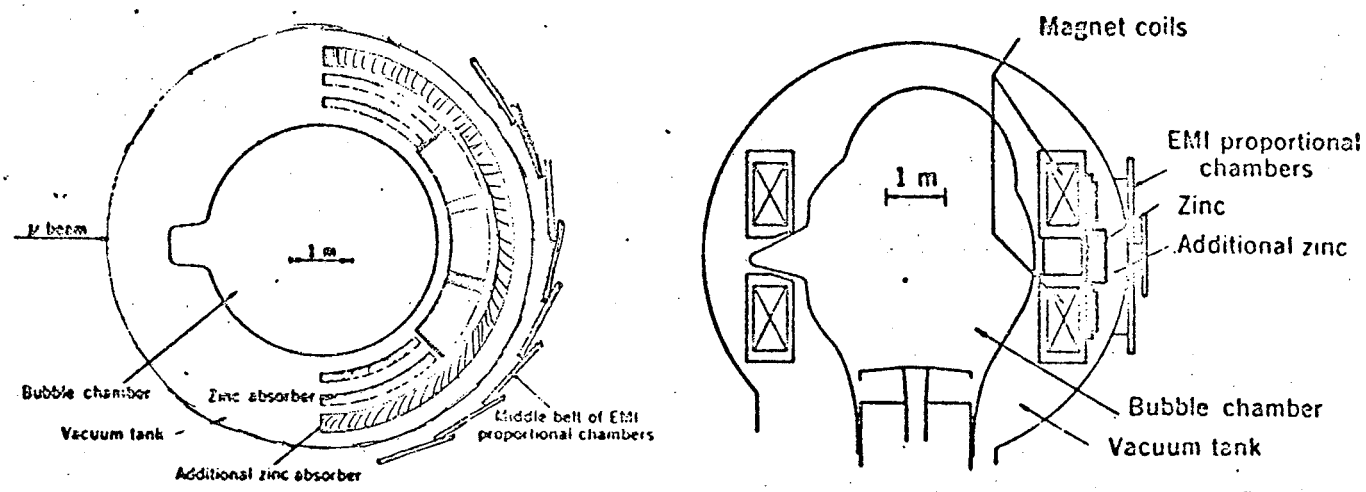

(b)

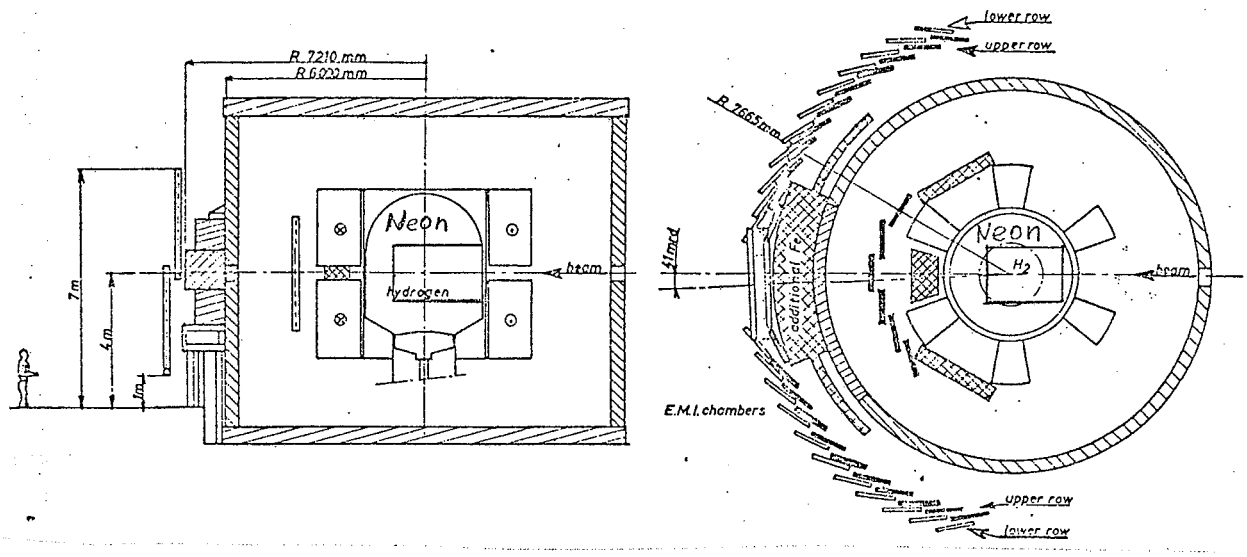

Fig. 20 (a) FNAL - 15 foot - Bubble Chamber with external muon identifier (EMI).

(b) BEBC (Big European Bubble Chamber) at CERN with Track Sensitive Target (TST) and EMI.

TABLE III

(a) Bubble chambers as ν-detectors

Name	Laboratory	Dimensions	Volume m^3 (fid.)	Magn. field kG	liquids used
1.2 HLB	CERN 63-65	1.15 Ø x .5 deep	0.5 (0.27)	27	freon (CF_3Br)
	CERN 67	1.15 Ø x 1 deep	1.13 (0.66)	27	propane (C_3H_8)
7 foot	BNL 70	2.1 Ø x 2.5 high	8 (?)	18	H_2, D_2
12 foot	ANL 72	3.8 Ø x 1.9 high	20 (11)	18	H_2, D_2
Gargamelle	CERN 71-75 (SPS 1977)	1.9 Ø x 4.8 long	12 (6 or 3)	20	freon propane
15 foot	FNAL 74	3.8 Ø sphere	30 (19)	30	H_2, Ne/H_2
SKAT	Serpukhov 1975	4.5 x 1.5 x 1	6.5 (?)	25	freon propane
BEBC	CERN/SPS 1976	3.7 Ø x 2 high	30 (18)	35	Ne, H_2, D_2

(b) Properties of bubble chamber liquids

	density g/cm^3	radiation length cm	nuclear collision length (cm)
H_2	0.063	1000	∿ 690
D_2	0.14	900	∿ 322
Ne (21% at.)/H_2	0.27	115	∿ 100
C_3H_8 (propane)	0.41	111	∿ 134
Ne	1.2	24	∿ 54
CF_3Fr (freon)	1.5	11	∿ 50

gamma conversion and neutron detection, some muon/hadron distinction due to the shorter hadron interaction length (but EMI also needed) and up to about 1 GeV pion/proton distinction due to the difference in ionization loss, but the neutrinos interact with nucleons bound in nuclei and hence the kinematics of the interaction is obscured.

K^+, K^- detection is only possible in case of characteristic decays and hence restricted to low energy kaons. The kinematics of neutrino interactions remain largely undetermined in case of outgoing neutrals (like in neutral current interactions with outgoing neutrinos).

2.3.3 Spark chambers, counter arrangements, calorimeters [39]

Spark chambers (for photographic track registration) or drift or multiwire proportional chambers (for electronic track registration and event analysis on-line) are sandwiched with high density material (iron plates, sometimes magnetized) to form large mass neutrino detectors (30-100 t, c.f. table IV, in the present counter experiment at the CERN SPS 1400 t). These detectors (example in fig. 21) allow - depending on their design and trigger logic - large event rates, good muon/hadron distinction, good total energy measurement (calorimeter principle), but poor vertex visibility, no gamma-electron distinction and neutrino interactions only on bound nuclei.

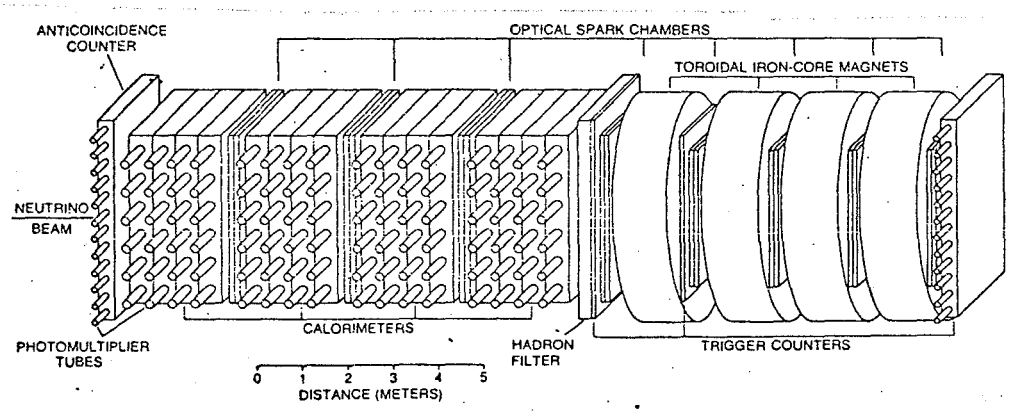

Fig. 21 FNAL-experiment 1A detector.

2.3.4 Nuclear emulsions [40]

Nuclear emulsions have highest spatial resolution (several microns, compared to 100-300 μ in bubble chambers) and can be used for the detection of short lived neutral particles ($\tau \approx 10^{-13}$ s). Only small masses can be processed and scanning for events is tedious.

2.4 List of neutrino experiments 1961-1976

Table IV lists the neutrino experiments at the accelerators of Argonne National Laboratory (ANL) (12 GeV), CERN (26 GeV), Brookhaven National Laboratory (BNL) (30 GeV), Serpukhov (70 GeV) and Fermi National Accelerator Laboraboratory (FNAL) (400 GeV) since 1961, indicating the main beam features, the detector type (B = bubble chamber, S = spark chamber-counter set-up) and the main topics studied (which will be treated in sect. 3).

Fig. 22 shows the layout of the CERN SPS and the location of the next series of ν-experiments at 400 GeV having just started.

Table IV

Accelerator ν-experiments until 1976

Accelerator	Year	Primary proton beam: energy (GeV)	Primary proton beam: intensity (10^{11} ppp)	Primary proton beam: total Nr (in 10^{17})	Neutrino beam: π,K focusing	Neutrino beam: spectrum determin.	Detector: type	Detector: mass (t)	Detector: material	TOTAL NUMBER OF EVENTS	Main results
BNL	61	15	3	3.5	-	from π,K	S	10	Al	∿ 50 ν	$\nu_\mu \neq \nu_e$
	63	30	3	1.2	1 horn	"	S	67	Al		1 π
CERN	63/4	25	3-6	7.6	"	"	B	.75	freon	∿ 450 ν	$\sigma(\nu n \to \mu^- p)$, M_A
CERN	63-4	25	3-6	3.9/3.7	"	"	S	65/90	Al, brass	∿ 10^4 ν	$m_w > 2$ GeV
CERN	65	25	7	3	"	"	B	1.8	freon	∿ 25 $\bar{\nu}$	$\sigma^{\Delta s=1} \lesssim \sigma^{Cabibbo}$
ANL	65	12	10	3	"	"	S	33	Al, FC		$\sigma(\nu n \to \mu^- p)$, M_A
CERN	67	21	7	7	horn + 2 refl.	from μ flux	B	.5	C_3H_8	∿ 450 ν	$\sigma(\nu p \to \mu^- N^{*++})$ $\sigma_{tot} \sim E$
	67	21	7	7	"	"	S	13	C, Al, Fe, Pb	∿ 10^4	L_μ conservation $\sigma^\nu = f(A)$
ANL	71	12	11	8	1 horn	from π,K	B	1.6 H_2 3.2 D_2			σ_{el}, NC
CERN	71-75	26	10-70	∿ 20	1 horn + 1 refl.	from μ flux	B	12	freon	∿ 10^4 ν	σ_{tot}, NC, $\mu^- e^+$
				∿ 50						∿ 4.10^4 $\bar{\nu}$	σ_{tot}, NC, $\bar{\nu}_\mu e^- \to \bar{\nu}_\mu e^-$
CERN	74/5	26	40-70		"	"	B	4	C_3H_8	ν,$\bar{\nu}$	in progress
	74/5	26	40-70		"	"	S	30	Al	∿4.10^5 ν,$\bar{\nu}$	NC π^o, $\nu_\mu e^-$
FNAL-WB	72-75	300-400	20-130		1 horn	from π,K	S	∿ 90	liqu. scin. and steel	ν,$\bar{\nu}$	2μ, NC, σ_{tot}
FNAL-NB	72-75	"			quadrupoles	"	S	∿ 30	steel	ν,$\bar{\nu}$	2μ, NC, σ_{tot}
FNAL-I5'	74-75	"			1 & 2 horns	"	B	1	H_2	1500 ν,$\bar{\nu}$	NC
FNAL-15'	75	300	∿ 10	∿ 10	1 horn	"	B	5	N_e/H_2	5000 ν	$\mu^- e^+$, in progress
FNAL-15'	76	400			2 horns	"	B	12	Ne	ν	in progress
SERP.	75-76	70	10							ν	in progress

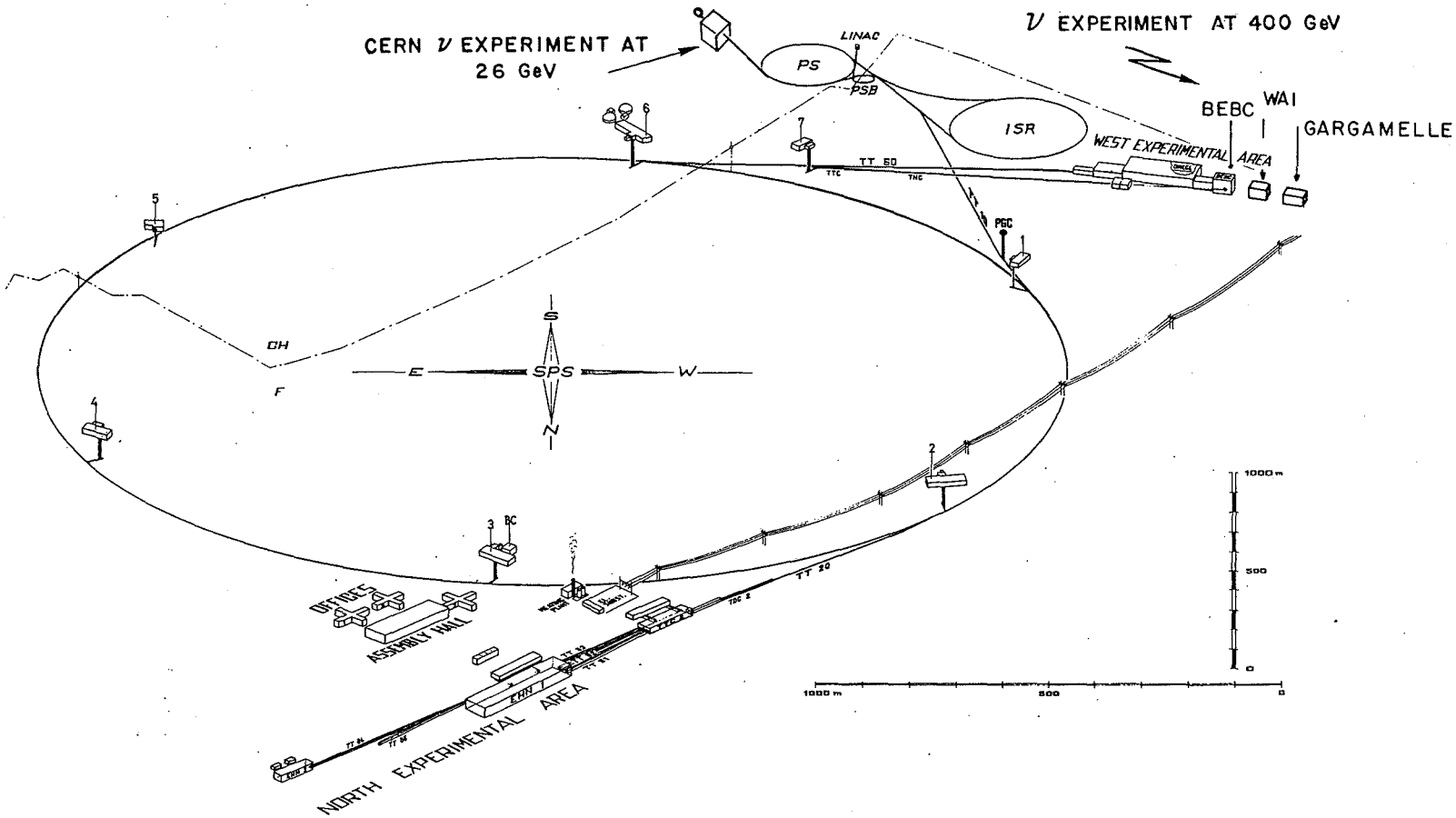
CERN ν EXPERIMENT AT
26 GeV
ν EXPERIMENT AT 400 GeV
LINAC
PS
PSB
ISR
BEBC
WAI
GARGAMELLE
WEST EXPERIMENTAL AREA
TT 60
PGC
CH
F
E
SPS
W
S
N
BC
OFFICES
ASSEMBLY HALL
EHN 1
TT 20
NORTH EXPERIMENTAL AREA
1000 m
500
0

Fig. 22

3. ν-NUMEROLOGY

Any event induced by neutral (non visible) particles in a detector exposed to a neutrino beam is a candidate for a neutrino interaction. There is strong evidence for these events to be neutrino events from their spatial and (in time recording electronic detectors) time distribution: the radial distribution is as expected from beam calculations, the flat longitudinal distribution corresponds to an infinitely long interaction length, the time distribution reflects the proton beam time structure.

From counting the neutrino events of certain topologies found on the bubble chamber or spark chamber film as a function of the event energy and knowing the neutrino spectrum one obtains cross sections for various interaction types (table V):

TABLE V

ν-beam		$\bar{\nu}$-beam		Numbers to measure, hypotheses to check
leptons	hadrons	leptons	hadrons	
μ^-	p	μ^+	n	Quasi-elastic ν-scattering $\nu + N \to \mu + N'$, nucleon is not a point as assumed in eq. 9, but has a structure measured as a form factor.
μ^-	$\Lambda\pi^+$	μ^+	Λ	$\lvert\Delta S\rvert = 1$ process. Cross section measures Cabbibo angle (spect. 1.6). $\mu^-\Lambda\pi^+$ checks $\Delta S = \Delta Q$ rule (p. 12)
μ^-	any	μ^+	any	Total cross section, checks quark parton model (p. 14)
e^-	any	e^+	any	Excess over beam expected rate (table II) checks lepton number conservation (p. 11)
e^-	0	e^-	0	Elastic ν-scattering $\nu_\mu e^- \to \nu_\mu e^-$, neutral current interaction (p. 15), measures Weinberg angle (p. 18)
0	p	0	p	Elastic neutral current interaction with nucleon $\nu p \to \nu p$, $\nu n \to \nu n$
0	any	0	any	Inelastic neutral current interaction $\nu N \to \nu N'$
$\mu^-\mu^+$	any	$\mu^+\mu^-$	any	Checks presence of charmed quark (sect. 1.9, p. 20) or of new leptonic particles
μ^-e^+	any	μ^+e^-	any	
> 2	any	> 2	any	More quarks? Heavy leptons?

How to single out the various types of interactions from other interactions and from background and how to extract the numbers necessary for the development of theory, is the subject of this section.

3.1 Charged current interactions ($\nu \to \ell^{\pm}$)

3.1.1 Quasi-elastic interactions $\nu + N \to \mu + N'$

Events are supposed to correspond to

$\nu + n \to \mu^- + p$ in ν beams,
$\bar{\nu} + p \to \mu^+ + n$ in $\bar{\nu}$ beams,

if they have the following topology:

ν	$\bar{\nu}$
one μ^- candidate one "fast" proton (kinetic energy T > 30 MeV)	one μ^+ candidate one "fast" neutron
any number of low energy nucleons, T < 30 MeV, if the target nucleon is bound in heavy nuclei.	

A muon candidate is a particle leaving the detector without having undergone a visible strong interaction. Neutrino energy and four-momentum transfer q (fig. 23) are determined from the energy of all final state particles (from curvature or range measurement).

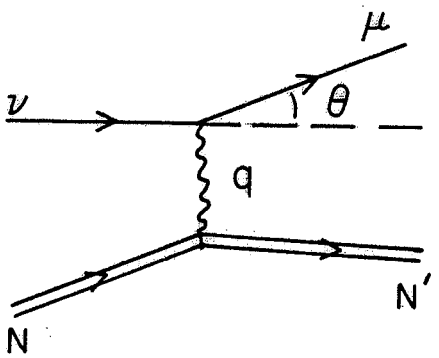

$$E_\nu = E_\mu + E_{N'}$$
$$q^2 = (p_\nu - p_\mu)^2$$
$$= 2(E_\nu E_\mu - p_\nu p_\mu \cos\theta - m_\mu^2)$$
$$\approx 4E_\nu E_\mu \sin^2(\theta/2)$$

Fig. 23 Kinematics of neutrino interaction, if Fermi motion of the target nucleon is neglected.

In order to reduce background events in the selected sample, cuts are applied: the events must be inside a well measurable (fiducial) volume, have more than a certain minimum energy (also because of larger spectrum uncertainty at low energy), and more than a minimum total forward momentum p_x (charged hadrons entering the detector from the side simulating ν-events have usually small p_x (fig. 24). Other background sources like $\nu N \rightarrow \nu\pi^- p$, where π^- leaves the detector without interaction or $\nu N \rightarrow \mu N'\pi$, where the π is absorbed in the nucleus, must be statistically corrected for (few per cent). Fermi motion of the target nucleon and the Pauli exclusion principle in the target nucleus complicate further the analysis of this interaction in heavy liquid bubble chambers [41] or in spark chambers [42]. In the 12' bubble chamber at ANL the quasi-elastic interactions were analysed in H_2 and D_2 [43]. The resulting cross section as a function of neutrino energy E_ν is shown in fig. 25.

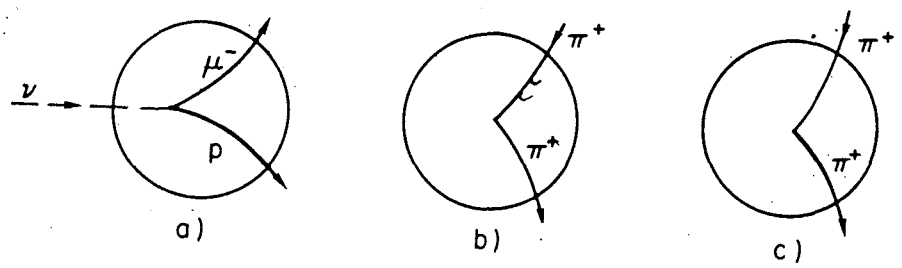

Fig. 24 (a) Quasi-elastic neutrino event.
(b) Incoming π^+ scattering, direction of flight signed by delta rays.
(c) Incoming π^+, direction not signed.

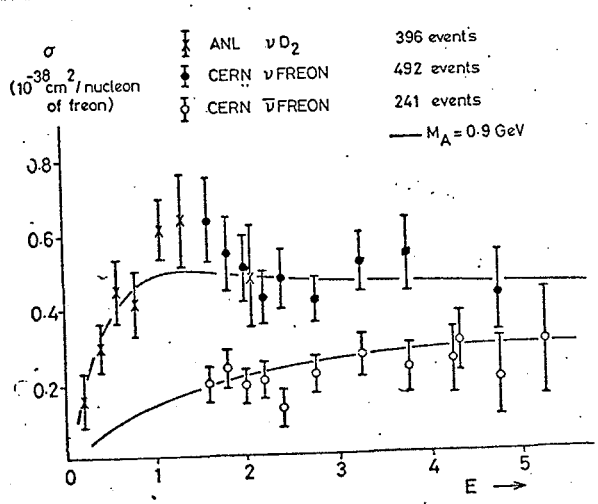

Fig. 25 Elastic cross sections $\sigma(\nu + n \rightarrow \mu^- + p)$ and $\sigma(\bar{\nu} + p \rightarrow \mu^+ + n)$ as determined at ANL and CERN.

The fact that it does not show the linear increase with energy as given by eq. (10) is due to the nucleon structure.

In order to calculate the theoretical cross section for this process, the (V-A)-matrix element (9) has to be extended to its most general Lorentz invariant expression, which might be written like this [44]:

$$\mathcal{M} = \frac{G}{\sqrt{2}} \left\{ \mu^- \gamma_\alpha (1+\gamma_5) \nu_\mu \right\} \quad \left\{ \bar{p} (V_\alpha + \gamma_5 A_\alpha) n \right\} , \tag{17(a)}$$

where

$$V_\alpha = \gamma_\alpha g_V + i(p_p + p_n) f_V + i q_\alpha h_V \tag{17(b)}$$

$$A_\alpha = \gamma_\alpha g_A + i(p_p + p_n) f_A + i q_\alpha h_A \tag{17(c)}$$

are the vector and axial vector part of the weak hadronic current and the six form-factors $g_{V,A}$ $f_{V,A}$ and $h_{V,A}$ contain the dynamics of strong interactions. We can now use some hypotheses about the hadronic weak current to reduce the number of form factors to be measured to one: (i) assuming <u>time reversal invariance</u> they must be all real; (ii) <u>G-parity conservation</u> (invariance under $G = Ce^{i\pi I_2}$, C = charge conjugation operator and I_2 = rotation by 180° around second axis of isospin) implies existence of so-called first class currents only, namely those parts of V_α transforming like $GV_\alpha G^{-1} = V^\alpha$ and of A_α transforming like $G A_\alpha G^{-1} = -A^\alpha$, which in turn implies $f_A = h_V = 0$; (iii) <u>hypothesis of conserved isovector current</u>. In sect. 1.2 we saw that weak interactions are universal, i.e. have the same coupling constant; consider especially the coupling constant for the pure <u>vector</u> transition $^{14}O \to {}^{14}N$ which is equal to that of μ-decay; this reminds of the remarkable fact that the absolute value of the proton charge is equal to the electron charge which corresponds to the conservation of the electromagnetic current and leads to the hypothesis that the weak hadronic vector current V_α is conserved. And since V_α does nothing else but turn a proton into a neutron ($^{14}_{8}O \to {}^{14}_{7}N$, $\Delta I = 1$), it must be an I = 1 object: $\vec{V}_\alpha = (V_{\alpha 1}, V_{\alpha 2}, V_{\alpha 3})$ with $V^{n \rightleftarrows p} = V_{\alpha 1} \mp i V_{\alpha 2}$. Then, $V_{\alpha 3}$ is a conserved isovector neutral current connecting p with p and n with n, which is the well known electromagnetic current. So, having the electromagnetic current and the weak hadronic current as members of the same

isotriplet, allows one to assume that also the form factors of the weak hadron current are the same as those of the electromagnetic hadron current and hence, are related to the electric and magnetic form factors F_Q and F_M in the Rosenbluth-formula by

$$g_V = F_Q(q^2) + (\mu_p - \mu_n)\, F_M(q^2)$$
$$f_V = \frac{\mu_p - \mu_n}{2m}\, F_M(q^2), \tag{18}$$

whence the term "weak magnetism" for f_V. $\mu_p = 1.52$ and $\mu_n = -1.79$ are the magnetic moments of proton and neutron, respectively, in Bohr magnetons.

(iv) <u>hypothesis of Partially Conserved Axial vector Current (PCAC)</u>. The axial vector current A_α, cannot be conserved (otherwise the π could not decay: $\delta A_\alpha/\delta x_\alpha = 0$), but partially, i.e. the form factor h_A is dominated by π exchange, which leads to a negligible contribution (2-3%) to the neutrino cross section, i.e. $h_A = 0$ (however, in μ capture it is measurable!).

So, eq. (17) reduces to

$$\mathscr{M} = \frac{G}{\sqrt{2}} \left(\mu\, \gamma_\alpha (1 + \gamma_5)\nu\right)\left(p\left[\gamma_\alpha\, g_V + (p_\alpha + n_\alpha)\, f_V + \gamma_\alpha\gamma_5\, g_A\right]n\right), \tag{19}$$

which leads to [45]

$$\frac{d\sigma^{\nu,\bar{\nu}}}{dq^2} = \frac{G^2}{4\pi}\left[A + B\,\frac{q^2}{E} + C\,\frac{q^2}{E^2}\right] \tag{20}$$

with

$$A = 2(g_A^2 + g_V^2) + (4m^2 + q^2)\, f_V^2 - 8m\, g_V\, f_V$$
$$B = -\frac{1}{m}\,(g_A \mp g_V)^2 - \frac{1}{m}\,(4m^2 + q^2)\, f_V^2 + 4\, g_V\, f_V$$
$$C = \frac{1}{2}\,(g_A^2 - g_V^2) + \frac{q^2}{4m^2}\,(g_A \mp g_V)^2 - \frac{1}{2}\,(4m^2 + q^2)\, f_V^2 + 2m\, g_V\, f_V\,,$$

where the only unknown quantity is the axial vector form factor $g_A(q^2)$. It is usually parametrized in the same way as F_Q and $F_M = F(q^2) = (1 + q^2/m_V^2)^{-2}$, namely

$$g_A(q^2) = g_A(0) \cdot (1 + q^2/m_A^2)^{-2} \tag{21}$$

and $g_A(0) = 1.23$ is obtained from neutron-β-decay. The interference term $\mp g_A g_V$ describes the difference between ν and $\bar{\nu}$ cross section (parity violation, corresponding to the pseudo-scalar of eq. (7)).

From fitting eq. (20) to the experimental cross sections (fig. 25) one obtains for M_A

	from $\sigma(E)$		from $d\sigma/dq^2$ (flux independent)		
	ν	$\bar{\nu}$	ν	$\bar{\nu}$	
CERN-Gargamelle	0.88 ± .19	0.69 ± .44	0.96 ± .16	0.94 ± .17	GeV/c^2
ANL - 12 ft	0.97 ± .16		0.94 ± .18		

which might be compared to the eN value for $M_V = 0.84$ GeV/c^2.

Eq. (20) shows that at $q^2 = 0$ and for $E_\nu \to \infty$ the ν and $\bar{\nu}$ elastic cross sections are equal

$$\frac{d\sigma}{dt}(q^2 = 0) = \frac{G^2}{2\pi}\left(g_A^2(0) + g_V^2(0) + 4m^2 f_V^2 - 4m\, g_V f_V\right) \tag{22}$$

$$= \frac{G^2}{2\pi}\left(g_A^2(0) + 1\right) = 0.4\, G^2 \approx 2 \times 10^{-38}\ \mathrm{cm}^2/(\mathrm{GeV/c})^2,$$

using eq. (18) at $q^2 = 0$

$$g_V(0) = 1 + \Delta\mu,\quad f_V(0) = \Delta\mu/2m$$

and $$g_A(0) = 1.23.$$

$d\sigma^{\nu,\bar{\nu}}/dt\ (E \to \infty) = (G^2/2\pi)A$ and, integrated, assuming the above parametrization for the form factor, $\sigma(\nu N \to \mu N', E \to \infty) \approx .7 \times 10^{-38}$ cm^2, a constant value, of which about 30% is due to weak magnetism.

A similar analysis of events selected for the topology $\mu^-\pi^+p$ yields information about the weak transition $p \to N^{*++}(\Delta 1232)$

$$\nu + p \rightarrow \mu^- + N^{*++}$$
$$\hookrightarrow p + \pi^+$$

which is the inverse N^{*++} β-decay. It is a SU_3 decuplet-SU_3 octet transition (fig. 3) and involves eight form factors. For details of the analysis and theoretical interpretation of the data (fig. 26) the reader is referred to the literature [45].

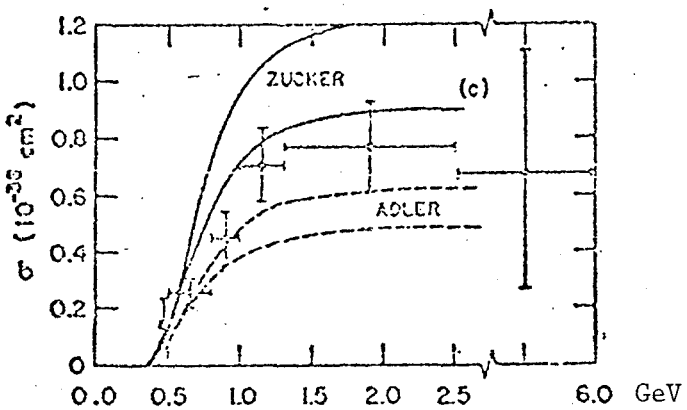

Fig. 26 $\nu + p \rightarrow \mu^- + \Delta^{++}$ cross section.

3.1.2 Strangeness changing processes

Some neutrino interactions (a few percent, increasing with energy) show a strange particle in the final state, i.e. a decay of a $\Lambda \rightarrow p\pi^-$, or a $K^o_s \rightarrow \pi^+\pi^-$, which are easily recognisable by their V shape topology. Many of these are due to associated production of two strange particles of opposite strangeness ($\Delta S = 0$ process), one of which is not detected (K^-, K^+ which look like π^-, π^+, or K^o_L which escapes). In the Gargamelle experiment [18] it has been tried to study the quasi-elastic process

$$\bar{\nu} + p \rightarrow \mu^+ + \Lambda$$

considering the following topologies:

	$\mu^+\Lambda$	$\mu^+ + \Lambda + p$ (<30MeV)	$\mu^+ + \Lambda + \gamma$	$\mu^+ + \Lambda + \pi, p$	$\mu^+ + Y + K$
Number obs.	10	3	2	5	8
most likely interpretation	$\Delta S = 1$	$\Delta S = 1$ and evaporation proton	$\Delta S = 1$ ($\Lambda\gamma = \Sigma^o$)	$\Delta S = 1$ inelastic or assoc. prod.	associated production

Taking the first two columns as quasi-elastic Λ-production, estimating from the last column the associated production background (1.5 ± 1.5 events), correcting for losses due to scanning (∿ 10%), short lifetimes (∿ 20% decay too close to vertex), unseen decay mode (33% $\Lambda \to \pi^o n$) one obtains 23^{+12}_{-5} single Λ-events. From these and the $\bar{\nu}$ flux a cross section of

$$\sigma(\bar{\nu} + p \to \mu^+ + \Lambda) = (1.3^{+.9}_{-.7}) = 10^{-40}\ cm^2/proton$$

is estimated assuming Λ-absorption and Σ^o-Λ conversion in the nucleus to cancel.

This is not in contradiction to the Cabibbo theory (sect. 1.6) [46]. An analysis using more statistics is in progress. In order to test the selection rules underlying the Cabibbo scheme eq. (12), more detailed experiments will have to be done.

3.1.3 Total neutrino cross sections: $\nu_\mu + N \to \mu$ + anything

These have been measured so far in three experiments (cf. table IV): in Gargamelle at CERN [22,47] from about 4000 ν and 3000 $\bar{\nu}$ events (between 1 and 15 GeV) and ν spectra measured via muon fluxes (sect. 2.2.5), in the 15 ft bubble chamber at FNAL [48] from about 1000 ν and 500 $\bar{\nu}$ events between 10 and 200 GeV and ν spectra calculated from predicted μ and K production data, and in spark chamber-calorimeter experiments [49-50] at FNAL. In order to arrive at the final result (October 1975 status is compiled in fig. 27), several corrections have to be applied depending on the type of experiment.

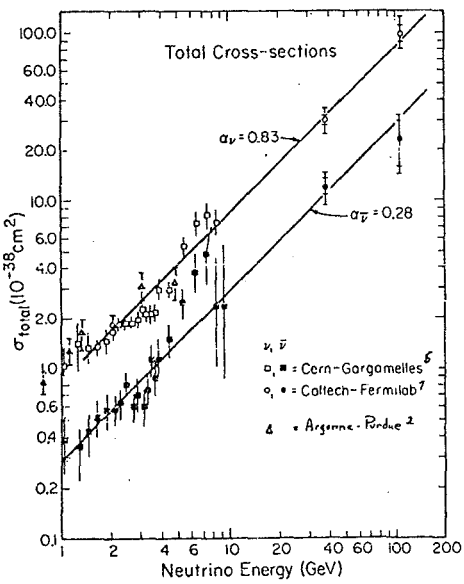

Fig. 27 Total cross sections for neutrinos and antineutrinos

In the Gargamelle experiment, for example, where the event energy is obtained from measuring the

momentum (by curvature or range) of all tracks, it has to be corrected for missing energy, the final event sample has to be corrected for background events from opposite sign neutrinos and neutral current interactions; in addition, the true energy distribution of events is distorted: due to the neutrino spectrum shape and the energy measurement error (∿ 15%) events are piled into the region of the spectrum bend from lower energies (fig. 28). This effect has to be folded out.

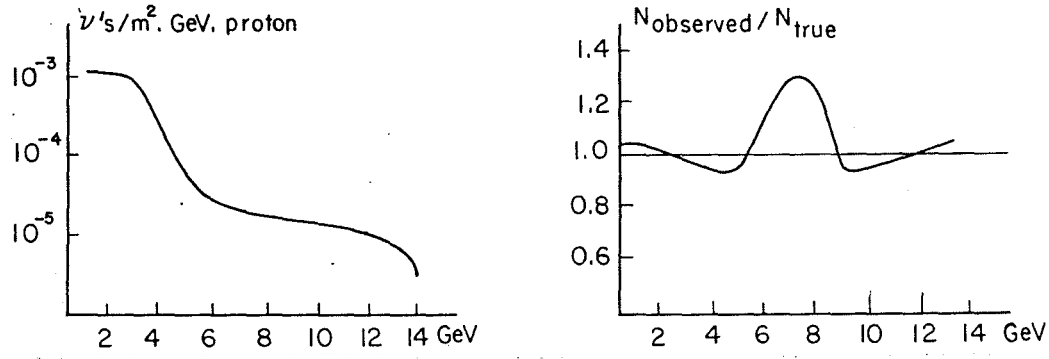

Fig. 28 Effect of neutrino spectrum shape and energy measurement error (∿ 15%) on the event distribution.

Cross sections from the Gargamelle experiment are still being analyzed, and new experiments (200 GeV narrow-band neutrino beam into neon filled BEBC and 1400 ton iron-scintillator calorimeter at CERN) are under way. Good evidence, however, from published results is that

$\sigma_{tot}^{\nu,\bar{\nu}}$ rise linearly with energy

and

$$\sigma^{\nu} = (.8 \pm .1) \times 10^{-38}\ E(\mathrm{GeV})\ \mathrm{cm}^2$$
$$\sigma^{\bar{\nu}} = (.3 \pm .05) \times 10^{-38}\ E(\mathrm{GeV})\ \mathrm{cm}^2 \qquad (23)$$
$$R = \sigma^{\bar{\nu}}/\sigma^{\nu} = .37.$$

What can be learnt from these numbers?

The most general expression for the total cross section is

$$\sigma^{\nu,\bar{\nu}} \sim G^2 \sum_{\text{spins}} \sum_{X} \left| \left(\mu\ \gamma_\alpha (1 + \gamma_5)\nu\right) \left(X|J_\alpha|N\right) \right|^2 \delta(p_N + p_V - p_X - p)$$

$$= G^2\ (\text{Lepton tensor } L_{\alpha\beta})(\text{Hadron tensor } H_{\alpha\beta}) \tag{24}$$

with the kinematical quantities defined in fig. 29.

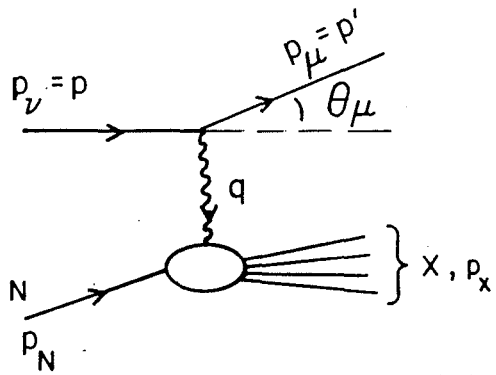

$q^2 = (p_V - p_\mu)^2 = 4\ EE_\mu\ \sin^2\theta_\mu$

$\nu = E - E_\mu = \frac{p \cdot q}{m}$

m = nucleon mass

Fig. 29 Kinematics of inelastic ν-scattering

$L_{\alpha\beta}$ is known (eq. (9))

$$= \bar{\Sigma}\Sigma\ j^*_\alpha\ j_\beta$$

$$= \text{Tr}\ \not{p}\ \gamma_\alpha (1+\gamma_5)(\not{p} + m_\mu)\gamma_\beta\ (1+\gamma_5)$$

$$= 8(p_\alpha\ p'_\beta + p_\beta\ p'_\alpha - p \cdot p'\ \delta_{\alpha\beta} + i_{\alpha\beta\rho\sigma}\ p_\rho\ p'_\sigma)$$

$H_{\alpha\beta}$ is unknown, and its most general Lorentz invariant form is [44(a) and 51]

$$= \delta_{\alpha\beta}\ W_1(q^2,\nu) + p_\alpha\ p_\beta\ W_2(q^2,\nu) - \frac{i}{2}\ \varepsilon_{\alpha\beta\rho\sigma}\ W_3(q^2,\nu)$$

+ terms which after contraction with $L_{\alpha\beta}$ are of order m_μ.

Both tensors contracted yields

$$\frac{d^2\sigma^{\nu,\bar{\nu}}}{dq^2 d\nu} = \frac{G^2}{2\pi m}\frac{E_\mu}{E}\left[W_1 \cdot 2 \cdot \sin^2\theta/2 + W_2 \cos^2\theta/2 \pm \frac{E+E_\mu}{m}\sin^2\theta/2 \cdot W_3\right]. \tag{25}$$

$W_{1,2,3}$ are structure functions and depend of the only two Lorentz scalars q^2 and ν. Their relation to the (real) form factors defined in the hadron current (before squaring) in the quasi-elastic case are

$$W_1 = g_A^2 + \frac{q^2}{4m^2}(g_A^2 + g_V^2)$$

$$W_2 = g_A^2 + (g_V - 2m\, f_V)^2 + q^2 f_V^2 \tag{26}$$

$$W_3 = -2\, g_A\, g_V \text{ (VA interference term!)} .$$

Charge symmetry requires

$$W_i^{\bar{\nu}p} = W_i^{\nu n}, \quad W_i^{\bar{\nu}n} = W_i^{\nu p} \tag{27}$$

Deep inelastic (large q^2, ν) scattering of electrons off nucleons has shown that νW_2 does not depend on q^2 and ν separately, but only on their ratio; that is scaling invariance (predicted by Bjorken). Defining

$$x = \frac{q^2}{2m\nu}, \quad y = \frac{\nu}{E}, \quad \text{i.e. } xy = \frac{2E_\mu}{m}\sin^2\theta/2 \tag{28}$$

and

$$W_1(q^2,\nu) \to F_1(x)$$
$$\frac{\nu W_{2,3}(q^2,\nu)}{m} \to F_{2,3}(x) \tag{29}$$

one can re-write eq. (25)

$$\frac{d^2\sigma^{\nu,\bar{\nu}}}{dxdy} = \frac{G^2ME}{\pi}\left[\frac{y^2}{2}(2x\, F_1(x)) + (1-y)\, F_2(x) \pm y(1-\frac{y}{2})(x\, F_3(x))\right], \tag{30}$$

which yields by integration a total cross section rising linearly with E

$$\sigma^{\nu,\bar{\nu}} = \frac{G^2ME}{\pi}\left\{\frac{1}{6}\int 2xF_1(x)dx + \frac{1}{2}\int F_2(x)dx \pm \frac{1}{3}\int xF_3(x)dx\right\} \tag{31}$$

$$= \frac{G^2mE}{6\pi}\int F_2(x)dx\,[3 + A \pm 2\,B] .$$

Using the numerical results of eq. (23) one finds

from $\sigma^{\nu} - \sigma^{\bar{\nu}} = \frac{G^2 mE}{\pi} \cdot \frac{2}{3} \cdot \int xF_3(x)dx$

$$\int xF_3(x)dx = 0.5 \pm .03 = B \int F_2 dx \tag{32}$$

and from

$$\begin{aligned} \sigma^{\nu} + \sigma^{\bar{\nu}} &= \frac{G^2 mE}{\pi} \left(\frac{1}{3} \int 2xF_1 + \int F_2 \right) \\ &= \frac{G^2 mE}{\pi} \int F_2(x)dx \left(1 + \frac{1}{3} A \right) \end{aligned} \tag{33}$$

together with

$$R = \frac{\sigma^{\bar{\nu}}}{\sigma^{\nu}} = \frac{3 + A - 2B}{3 + A - 2B} = .37, \text{ i.e.} \tag{34}$$

$(.9 \pm .04) \leqslant A \leqslant 1$, which means

$$\int F_2(x)dx \approx \int 2xF_1(x)dx, \tag{35}$$

the following bounds for $\int F_2(x)dx$

$$(.54 \pm .03) \leqslant \int F_2(x)dx \leqslant (.56 \pm .03). \tag{36}$$

The structure functions obtain a descriptive interpretation in the quark parton model (p. 14), which in its "naive" form states that the nucleon consists of quasi-free point-like constituents of a defined small mass with momentum $x \cdot p_N$, which have the quark properties (p. 20). The scaling variable x is then the fraction of the nucleon momentum carried by one quark and ν scattering happens on the quarks Q_i (fig. 30).

$$\begin{aligned} (xp_N)^2 &= (q + xp_N)^2 \\ &= q^2 + 2xp_N \cdot q + (xp_N)^2 \end{aligned}$$

which yields with $\nu m = pq$ (fig. 28)

$$x = q^2/2m\nu$$

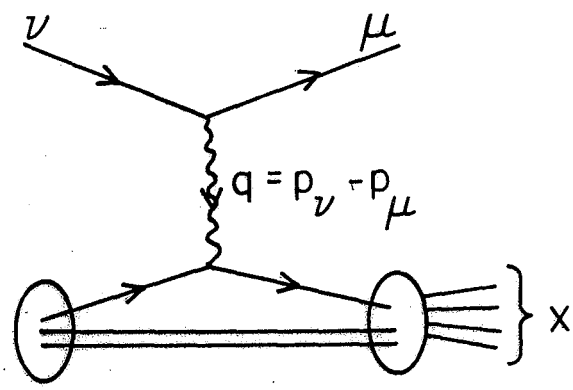

Fig. 30 Interpretation of x in quark parton model.

For these interactions the cross section formulae for point-like fermion (p. 9) apply

$$\frac{d\sigma^{\nu Q}}{dy} = \frac{G^2}{\pi} s^{\nu Q} = \frac{G^2}{\pi} x\, s^{\nu p} = \frac{2G^2 mE}{\pi} x$$

$$\frac{d\sigma^{\bar{\nu} Q}}{dy} = \frac{G^2}{\pi} s^{\bar{\nu} Q}(1-y)^2 = \frac{G^2}{\pi} x\, s^{\bar{\nu} p}(1-y)^2 = \frac{2G^2 mE}{\pi} x\, (1-y)^2 \tag{37}$$

ant the cross sections for ν-scattering off nucleons (p,n) become

$$\frac{d\sigma^{\nu p}}{dxdy} = \sum_i \frac{d\sigma^{\nu Q_i}}{dy} Q_i(x) + \sum_i \frac{d\sigma^{\nu \bar{Q}_i}}{dy} \bar{Q}_i(x)$$

$$\frac{2G^2 mE}{\pi} x \sum_i [Q_i(x) + \bar{Q}_i(x)(1-y)^2] \tag{38}$$

$$\frac{d\sigma^{\bar{\nu} p}}{dxdy} = \frac{2G^2 mE}{\pi} x \sum_i [\bar{Q}_i(x) + Q_i(x)\ (1-y)^2],$$

where $Q_i(x), (\bar{Q}_i(x))$ are the probabilities to find quarks (antiquarks) of type i with momentum xp_N and mass xm.

On the other hand, eq. (30) becomes with eq. (35)

$$\frac{d^2\sigma^{\nu,\bar{\nu}}}{dxdy} = \frac{G^2 mE}{2\pi} \left[(F_2 \pm xF_3) + (F_2 \mp xF_3)(1-y)^2\right] \tag{39}$$

and by comparison with eq. (38), F_2 and xF_3 can be interpreted as

$$F_2(x) = 2\, x\, Q_i(x) + 2\, x\, \bar{Q}_i(x)$$

$$xF_3(x) = 2\, x\, Q_i(x) - 2\, x\, \bar{Q}_i(x)\ ,$$

i.e., as the sum and the difference of parton and antiparton densities.

Without going into further detail the following conclusions can be drawn from the numbers (23) within the context of this picture

(a) From the near equality of eqs (32) and (36)

$$\frac{\bar{Q}_i}{Q_i + \bar{Q}_i} = .05 \pm .02$$

i.e. there is nearly no antimatter in the nucleon.

(b) From comparing $\sigma^{\nu} + \sigma^{\bar{\nu}} \approx 1.1$ with $\int F_2 dx = \int x\,(Q + \bar{Q})dx \approx .55$, it follows that only half of the nucleon momentum is carried by charged partons. The other half is usually ascribed to quark binding neutral gluons.

(c) From the facts that the equivalent analysis for eN scattering shows the same result (i.e. that only half of the nucleon momentum is carried by active quarks), and electrons should also scatter off strange and charmed quarks (no $\sin^2\theta_c$-suppression), it can be concluded that there are also less than 10% λ and c quarks in matter.

(d) From eqs (37) and (38) and (a), it is expected that

$$\frac{d\sigma}{dy} \sim \begin{cases} \text{const for } \nu \\ (1-y)^2 \text{ for } \bar{\nu} \end{cases} .$$

However, a recent counter experiment at FNAL indicates deviations from this simple model: the total cross section ratio $\sigma^{\bar{\nu}}/\sigma^{\nu}$ seems to become significantly larger than 1/3 at higher energy (fig. 31 (a)) and the distribution in energy transfer from anti-neutrino to hadron does not seem to follow the simple law $d\sigma/dy \sim (1-y)^2$ at higher energies (fig. 31 (b) and (f)). See, however, ref. [52].

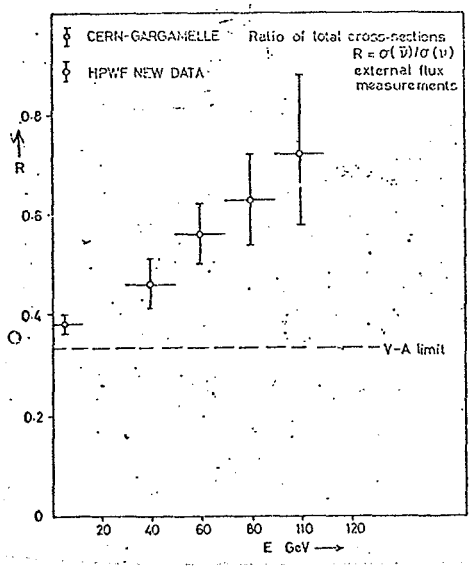

Fig. 31 (a) Total cross section ratio obtained in one of the counter experiments at FNAL (E1A).

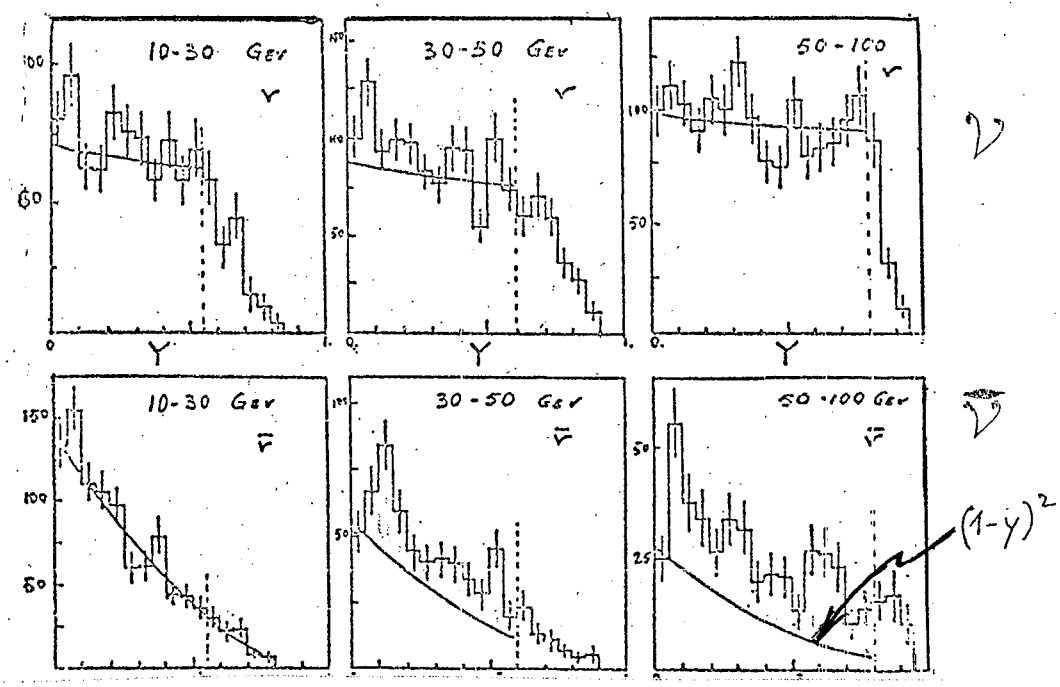

Fig. 31 (b) y-distributions (for x < .6) from experiment E1A.

3.1.4 Electron neutrino interactions: $\nu_e + N \to e +$ anything

From table II and fig. 15 it is expected that of the order of 1% of the interactions in a neutrino experiment should be induced by electron neutrinos and - according to sect. 1.5 - lead to electrons (ν_e) or positrons ($\bar{\nu}_e$) in the final state. At present, electrons are best identified in heavy liquid bubble chambers (sect. 2.3.2). In the Gargamelle (freon) neutrino experiments events with electrons (positrons) have been observed and analysed in terms of total cross sections. The first results [53] from about 50 e-events indicate that the total cross section for ν_e is the same as for ν_μ (in agreement with μ-e-universality). The number of events also agrees with muon number conservation (sect. 1.5), i.e. ν_μ do not turn into e. In addition, the e-events at low energy which are mainly induced by ν_e's from muon decay can be used to check whether the lepton number is conserved additively (allowing only $\mu^+ \to e^+ + \bar{\nu}_\mu + \nu_e$, hence only e^--events in neutrino beam) or multiplicatively (allowing also $\mu^+ \to e^+ + \nu_\mu + \bar{\nu}_e$, hence 50% e^- and 50% e^+ events at low energy). From the small number of events obtained so far complete multiplicativity can be excluded (but not a small admixture).

3.2 Neutral current interactions ($\nu \to \nu$)

3.2.1 $\bar{\nu}_\mu + e^- \to \bar{\nu}_\mu + e^-$

Two million pictures obtained with the CERN heavy liquid bubble chamber Gargamelle exposed to an antineutrino beam (using $4.7 \cdot 10^{18}$ protons) were double scanned for events showing nothing but a single electron. Three events were found [23], one of which is shown in fig. 32 (a).

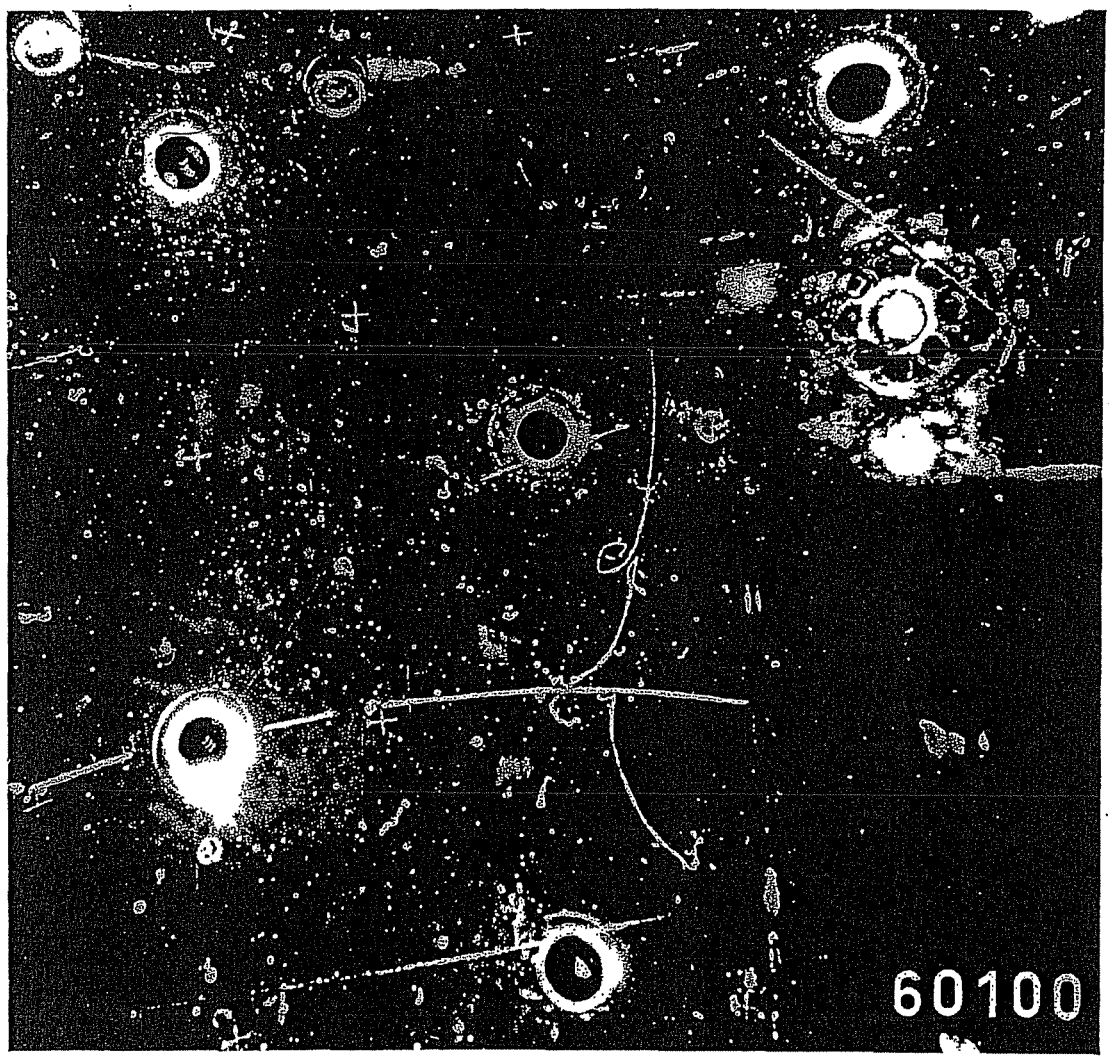

Fig. 32 (a) Single electron corresponding probably to $\bar{\nu}_\mu + e^- \to \bar{\nu}_\mu + e^-$.

Processes known so far which could produce single electrons, like

$\nu_e + N \to e^- + p$, p not visible

$\overset{(-)}{\nu}_e + e^- \to \overset{(-)}{\nu}_e + e^-$

$\gamma \to e^+e^-$ very asymmetrically (e^+ invisible)

$\gamma + e^- \to \gamma + e^-$ (Compton electron)

can at most account for 0.44 events. Therefore, and because the lepton number is conserved, it is concluded that the three events are due to the neutral current process (Z^o exchange, p. 15)

$$\bar{\nu}_\mu + e^- \to \bar{\nu}_\mu + e^- .$$

The three events, after background subtraction and correction for losses (e.g. electrons radiating so early that they look like converted gammas) correspond to a cross section $(.1^{+.21}_{-.09})\ E_{\bar{\nu}}$ (GeV) $.10^{-41}$ cm^2/electron. This can be analyzed in terms of the Weinberg model (p. 18), which predicts the following matrix element

$$\mathscr{M} = \frac{G}{\sqrt{2}} \left\{\bar{\nu}\ \gamma_\alpha\ (1 + \gamma_5)\nu\right\} \left\{\bar{e}\ \gamma_{\bar{\alpha}}(g_V + g_A\gamma_5)e\right\}$$

and hence

$$\frac{d\sigma}{dy} = \frac{G^2 m_e E_\nu}{2\pi} \left[(g_V - g_A)^2 + (1-y)^2\ (g_V + g_A)^2\right]$$

with $g_V = -\frac{1}{2} + 2\sin^2\theta$, $g_A = -\frac{1}{2}$. For the parameter θ (Weinberg angle) the following result is found: $0.1 < \sin^2\theta < 0.4$.

3.2.2 $\nu + N \to \nu +$ hadrons

In order to search for this process events have to be selected which have no charged lepton in the final state. Then, it has to be shown that these events are not induced by incoming neutral hadrons. This was done for the first time in 1973 in the Gargamelle neutrino experiment [24] at the CERN 26 GeV accelerator, and confirmed in a counter-spark chamber experiments [25] at the FNAL 300-400 GeV accelerator.

In heavy liquid bubble chamber the relatively short hadron interaction length (table III, Gargamelle was filled with freon) allows good muon/hadron distinction. About 20% of the interactions observed in the neutrino beam and about 40% in the antineutrino beam had no muon candidates (example in fig. 32 (b). How can one prove that these events are not induced by incoming

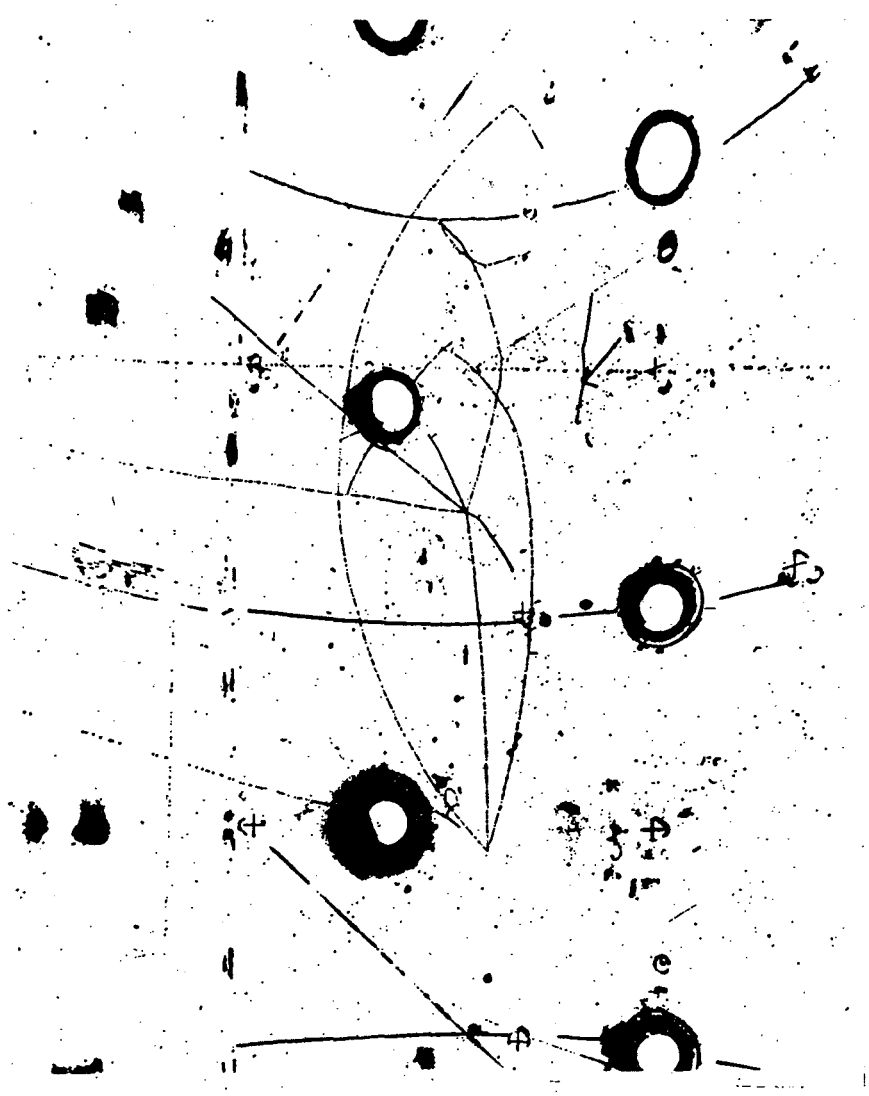

Fig. 32 (b) Example of hadronic neutral current interaction.

neutrons? Firstly, by the spatial distribution of the events. Neutron induced events would fall off exponentially, whereas the observed events have distributions similar to the charged current events (fig. 33).

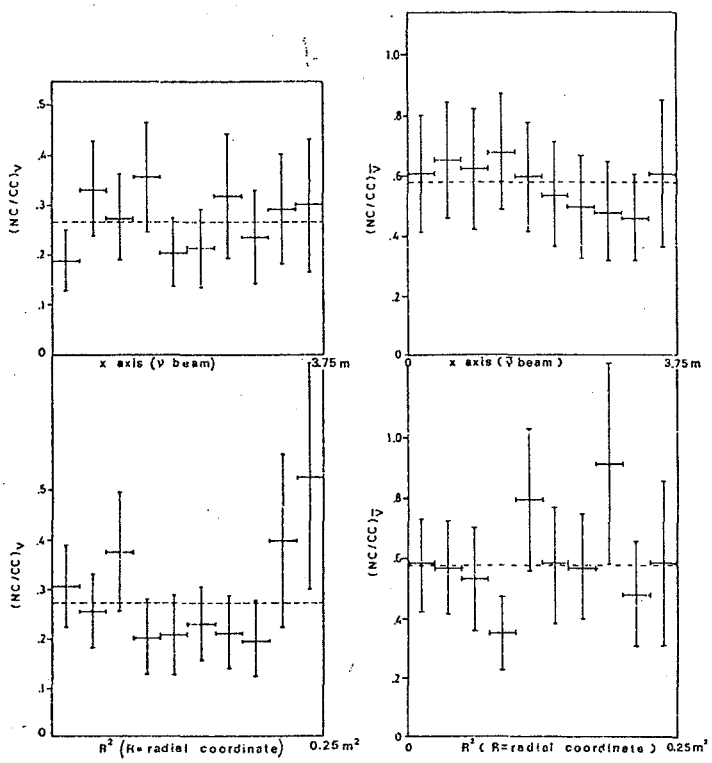

Fig. 33 Distribution in x (beam direction) and r^2 (r = distance from beam axis) of the neutral current events relative to the charged current events found in Gargamelle.

Secondly, by the energy distribution of the events. Neutron induced events would mainly come from neutrino produced neutrons, i.e. tertiary particles having a softer energy spectrum than neutrino induced events.

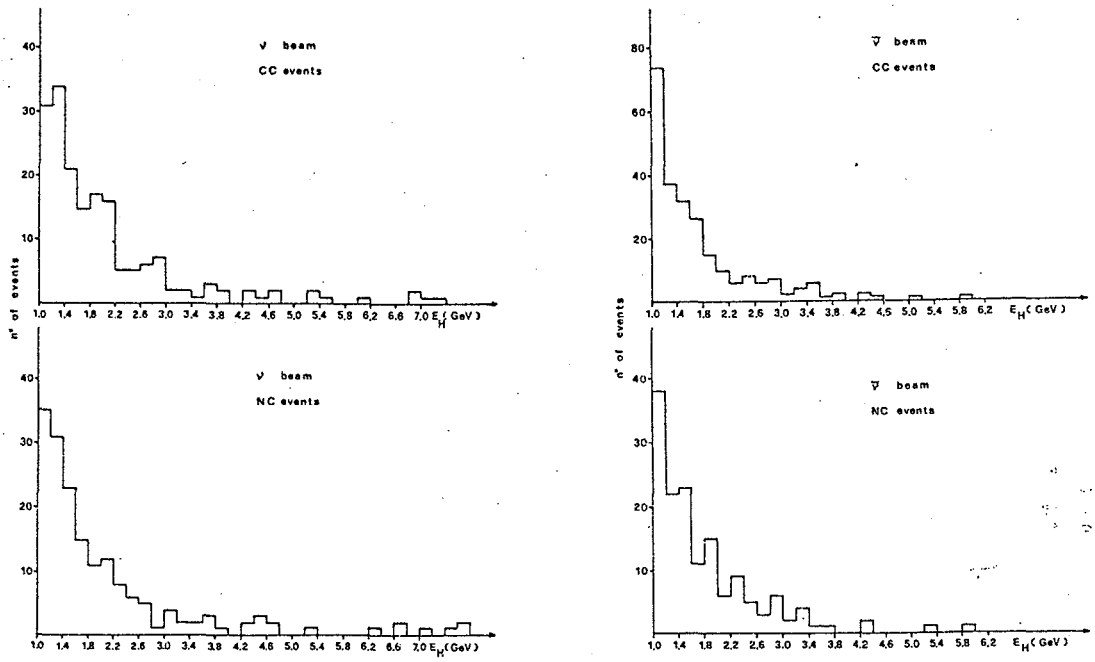

Fig. 34 Distributions of visible energy of the neutral current events and of the hadronic energy of the charged current events.

Fig. 34 demonstrates the similarity between the distribution of total visible energy of events without lepton candidate and that of hadronic energy (= total visible energy minus muon energy) of events with muon candidate. Fig. 34 suggests that in the events without a muon candidate the incoming neutrino transfers about the same energy to the hadronic system as in the events with a muon candidate and that in the first case it comes out of the interaction as a neutrino, in the second case as a muon.

Thirdly, by Monte-Carlo calculations of background from neutrons produced by neutrinos in the material around the bubble chamber, the only possible source of neutrons, since the beam region is well shielded. These calculations show that such background cannot account for more than 15-20% of the events with (hadronic) energy of more than 1 GeV.

The resulting ratios of neutral current (NC) to charged current (CC) interaction rates in neutrino (R_ν) and antineutrino ($R_{\bar\nu}$) beams can be analyzed in terms of the Weinberg-Salam model (p. 18) which describes the neutral current interaction by the matrix element

$$M = \frac{G}{\sqrt{2}} (\bar\nu \gamma_\alpha (1 + \gamma_5)\nu)(J^o_\alpha)$$

and

$$J^o_\alpha = J^3_\alpha - 2\sin^2\theta_W \cdot J^{el.m.}_\alpha =$$

$$= A^3_\alpha + (1 - 2\sin^2\theta_W) V^3_\alpha .$$

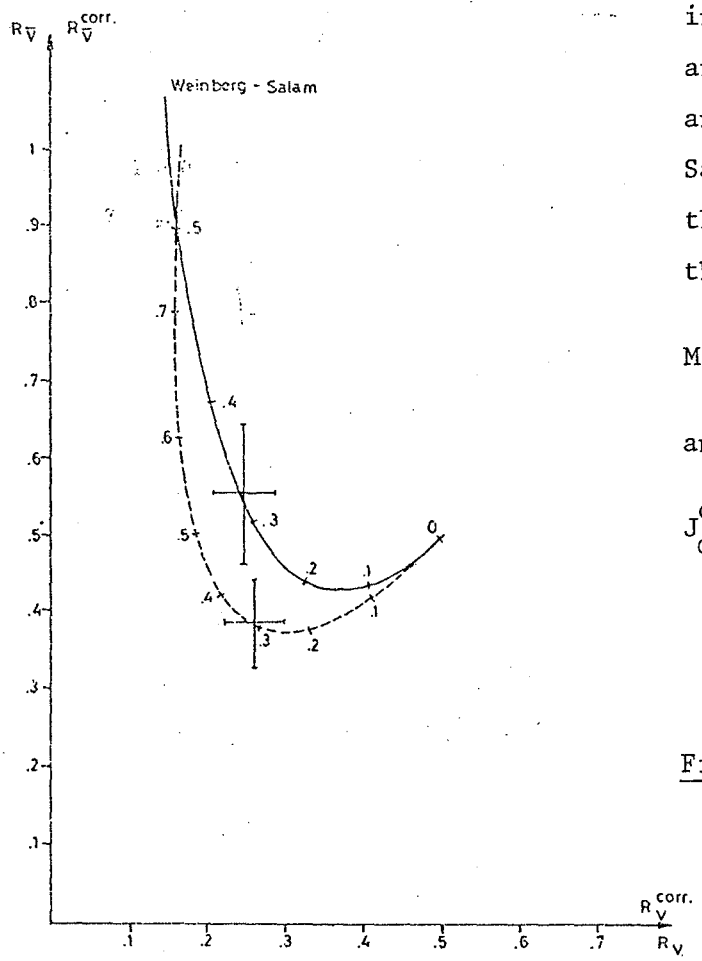

Fig. 35 Comparison of the NC/CC production ratios in ν and $\bar\nu$ interactions (upper cross without lower cross with correction for E_H cut at 1 GeV) with Weinberg-Salam model.

In order to compare the experimental NC/CC ratios $R_\nu = 0.25 \pm 0.04$ for neutrinos and 0.56 ± 0.10 for antineutrinos with this theory, corrections must be made for the 1 GeV cut in hadronic energy, and that is model dependent. Assuming scaling, V-A theory for CC, and neutrino scattering off point like, spin-½ quarks and using the results of sect. 3.2.3, the ratios become 0.26 ± 0.04 (ν) and 0.39 ± 0.06 ($\bar{\nu}$), without cut in hadronic energy. Table VI shows these results together with those of the two FNAL experiments. From a fit to the theoretical prediction (fig. 35), one obtains for the mixing parameter $\sin^2\theta_W \sim 1/3$, in agreement with the $\bar{\nu}_\mu e \to \bar{\nu}_\mu e$ result.

TABLE VI

NC/CC rates from various experiments in June 1976 [53]

Experiments	R^ν	$R^{\bar{\nu}}$	Remarks
Gargamelle	0.26 ± 0.04	0.39 ± 0.06	$\langle E \rangle \sim 2$ GeV, $E_h \gtrsim 1$ GeV
HPWF	0.29 ± 0.04	0.39 ± 0.10	$\langle E_\nu \rangle = 53$ GeV, $\langle E_{\bar{\nu}} \rangle \sim 11$ GeV, $E_h \gtrsim 4$ GeV
CITF	0.24 ± 0.04	0.35 ± 0.11	$\langle E \rangle \sim 50$ GeV, $E_h \gtrsim 12$ GeV

3.3 Two lepton events

3.3.1 Di-muon events in counter experiments

In the counter spark chamber arrangements of the FNAL-neutrino experiments in wide-band [55] and narrow-band [56] beams events with two muons in the final state were observed. The muons were identified by their penetration through many meters of iron (fig. 36).

The rate of these events is about 1% of the normal charged current events.

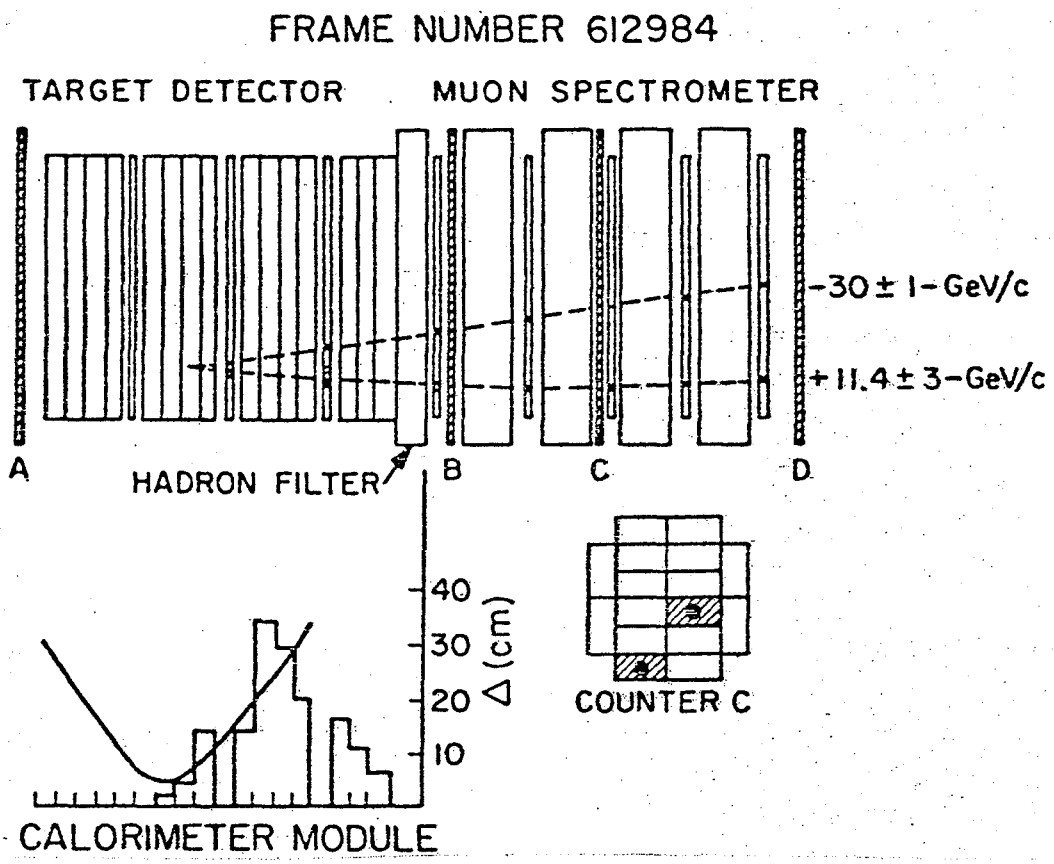

Fig. 36 Di-muon event from the "Harvard-Pennsylvania-Wisconsin-Fermilab Apparatus (fig. 21)

Processes simulating events with direct production of two-muons:

(a) Normal charged current events with one muon and one pion (or kaon) decaying into a muon without visible kink. By comparing the rate of 2-μ-events from regions of the detector with different density (i.e. different relative decay and interaction probabilities) this background can be estimated to be less than 25%.

(b) Neutral current interactions with one of the hadrons being a meson which decays into two muons (e.g. $\rho^o \rightarrow \mu^+\mu^-$). This can be excluded because the rate of such process would be much smaller and the invariant mass of the observed two-muon system is varying over several GeV.

RIT

Processes with direct production of two muons at the neutrino vertex could be:

(a) Production and leptonic decay of an intermediate vector boson (sect. 1.4):

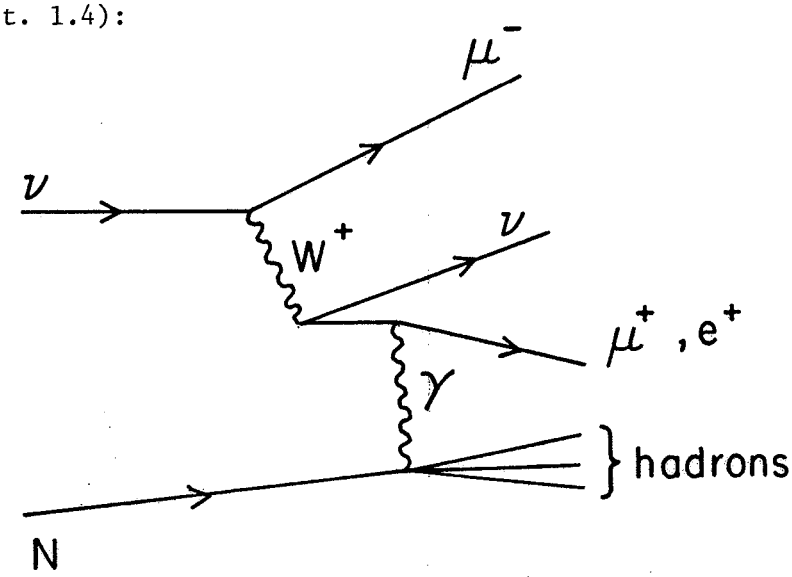

Fig. 37 (a) Production and decay of an intermediate vector boson.

Then, the μ^- and W^+ would be produced with small relative velocity (in their centre of momentum system) and have mean momenta (in the laboratory system) in the ratio of their masses, i.e. $\langle p_{\mu^-}\rangle \approx \langle p_{\mu^+}\rangle$, whereas the experimentally observed ratio is $\langle p_{\mu^-}\rangle/\langle p_{\mu^+}\rangle \sim 6$.

(b) Production and leptonic decay of a heavy lepton L^o (spin ½):

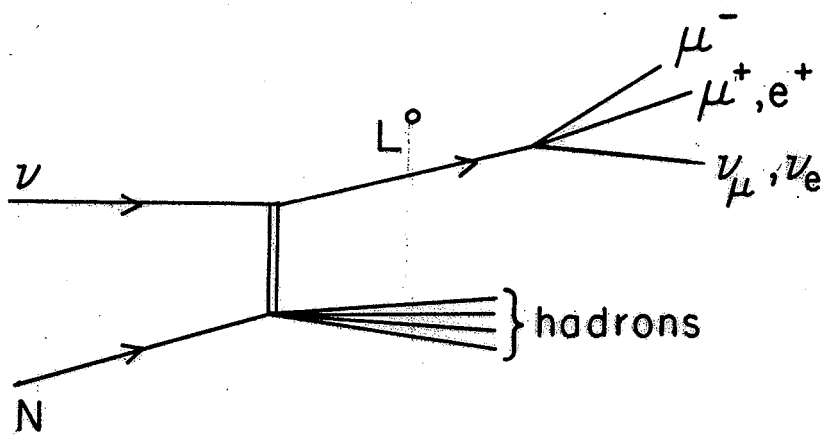

Fig. 37 (b) Production and decay of a heavy lepton.

In that case the average ratio of momenta must be between ½ and 2 [57], also in disagreement with the observation.

(c) Production and leptonic decay of a new hadron (Y) with a new hadronic quantum number (charm), in agreement with the scheme outlined in sect. 1.9:

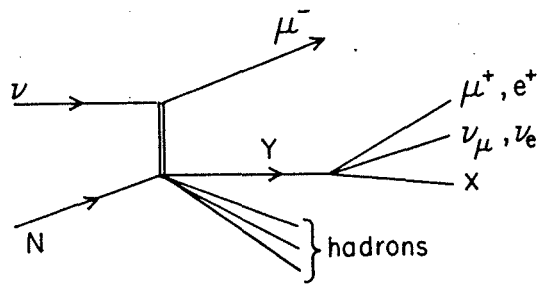

Fig. 38 Production and decay of a charmed hadron.

This interpretation is for the time being the most probable one and explains also the recent phenomena observed at e^+e^- storage ring experiment (J/ψ and D production at SLAC and DESY).

3.3.2 μ^-e^+ events in heavy liquid bubble chambers

Dilepton events have also been searched for in heavy liquid bubble chambers: in Gargamelle at CERN and in the 15' chamber at FNAL. In these experiments the second lepton which is searched for is a positron(*), since the short radiation length of heavy liquids allows good electron recognition already at the scanning stage:

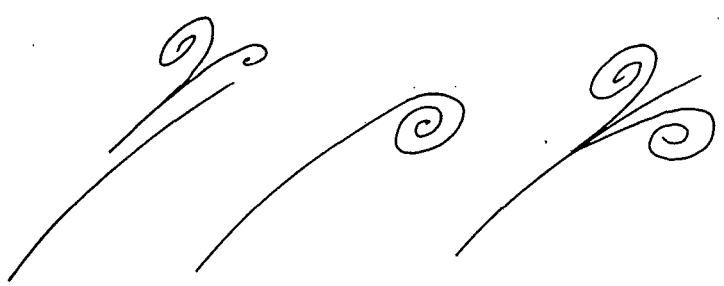

(a) bremsstrahlung (b) spiraling (c) direct pair-production

Fig. 39 Electron (positron) identification criteria.

(*) Di-muon search in the 15' chamber which has an EMI (sect. 2.3.2, fig. 20(a)) is in progress.

The other advantage of bubble chambers is to search also for strange particles which are expected if the dilepton events are due to charmed particle decay (sect. 1.9). The first event of this type was seen in Gargamelle [58(a)], the final sample [58(b)] is shown in table VII, together with the observations of the two 15' bubble chamber experiments [59]. Fig. 40 shows an example, where the particle X of fig. 38 is a K_s^o.

TABLE VII

μe events in 3 heavy liquid bubble chamber ν experiments (March 1977)

	Gargamelle freon	15' bubble chamber Ne (21%)/H_2	Ne (64%)/H_2
No. of photos	2 000 000	70 000	46 000
Charged current events	41 000	5400	30 000
$\mu^- e^+$ events	20	17	71
E_{e^+} cut (GeV)	.2	0.8	0.3
background	7	< 1	12 ± 9
losses due to cuts	< 1	< 1	7 ± 3.5
e detection efficiency	0.97 ± 0.02	0.36 ± 0.1	.64 ± 0.1
$\mu^- e^+/\mu^-$ (%)	0.3 ± 0.1	0.77 ± 0.3	0.5 ± 0.2
$\mu^- e^+ V^o/\mu^- e^+$	3/20	11/17	11/71

In order to arrive at the rates quoted in table VII, detection efficiencies for electrons, background and loss rates have to be estimated. The main background source for $\mu^- e^+$ events are Dalitz pairs ($\pi^o \to e^+ e^- \gamma$, 1.15% branching ratio) with one electron branch being so small that single electron production is simulated. Other sources are K_{e3} decays and $\bar{\nu}_e$ interactions. In all these experiments background interactions can only account for a few percent of the μe-events.

As in the case of the di-muon events the μe-events are most likely explained in terms of leptonic decay of charmed hadrons $c \to s + \ell^+ + \nu$.

HAUT

VOIR ANNEXE

Fig. 40

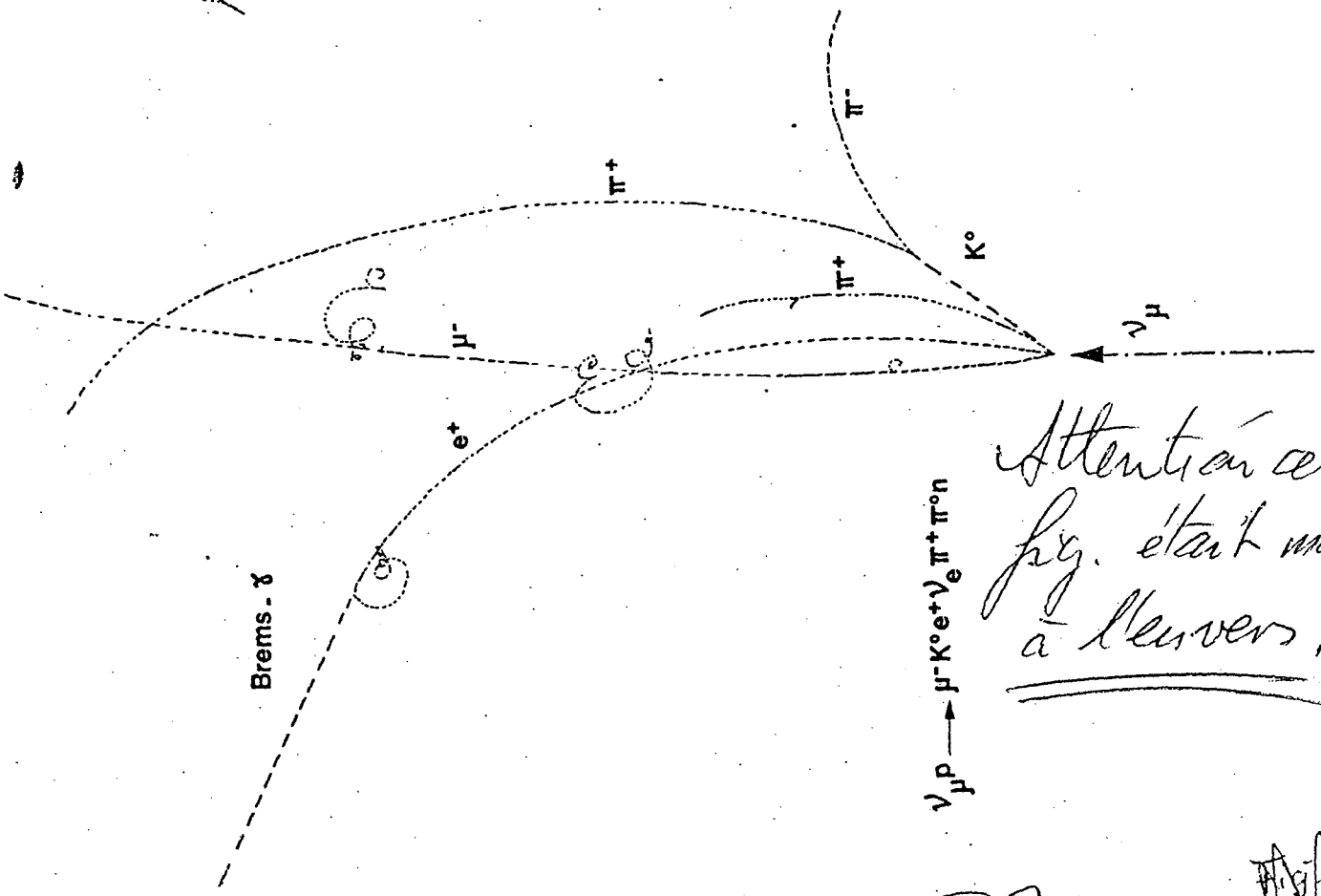

Attention cette fig. était montée à l'envers !

Fig. 46

The μe-events support further evidence for this hypothesis since they show strange particles at a higher rate than the "normal" charged current events. The only strange particles which are easily identifiable in bubble chambers are K_s^o and Λ by their neutral decay mode (V^o, p. 49). The discrepancy in V^o rates of the two 15' bubble chamber experiments is not fully understood and must be due to experimental biases and statistics.

The GIM [30] model (p. 19) predicts the production of one charmed particle off valence quarks according to fig. 8 (p. 21)

$$\nu + n \rightarrow c + \mu^- .$$

From the matrix element (fig. 7, p. 19)

$$M = (\mu\nu)(\lambda' c)$$

$$= (\mu\nu)\ [(-n\ .\ \sin\theta_c + \lambda\cos\theta_c)\ c]$$

it is also predicted that the rate of charmed particle production is suppressed by $\sin^2\theta_c$ with respect to the "normal" transition

$$M = (\mu\nu)(n' p)$$

$$= (\mu\nu)\ [(n\ \cos\theta_c + \lambda\sin\theta_c)\ p]$$

The leptonic decay of a charmed particle is described by

$$M = (\mu\nu)\ (\lambda' c) \text{ or } (e\nu)(\lambda' c)$$

$$= (e\nu)\ [(-n\ \sin\theta_c + \lambda\cos\theta_c)\ c]\ ,$$

i.e. a charmed particle decays preferentially ($\sim \cos^2\theta_c$) into a strange particle.

Hence - in this model - from the observed di-lepton rates of table VII and p. 68, it can be concluded that the leptonic branching ratio of charmed particles (produced at a rate of $\sin^2\theta \sim 5\%$) is somewhere between 10 and 20%.

However, further studies are necessary - especially of strange particle production in di-lepton events - before conclusions can be drawn about the extent of validity of this model.

CONCLUSIONS AND OUTLOOK

The concept of the lefthanded neutrino existing in two types (ν_e, ν_μ) and interacting via $W^\pm$ and/or Z^o exchange with pointlike quasi-free three-coloured four-flavoured (p,n,λ,c) constituents of (colourless) hadrons allows to describe nearly all phenomena classed as weak interactions, especially high energy neutrino interactions, the subject of these lectures. However, deviations from exact scaling - the structure function F_i, equ. (29), are not functions of x only but depend also on q^2 [60] - require extension of the theory. The existence of a third lepton type (called U or, now, τ) and lepton-hadron symmetry arguments suggest introduction of more quarks. Also CP violation cannot be accounted for by only four quarks. How many more quarks? One, two or three?

"Wo das Verstehen aufhört, fängt das Zählen an..."

Schopenhauer

(Where understanding ceases, counting starts)

APPENDIX A

MASS GENERATION BY SPONTANEOUS BREAKING OF GAUGE SYMMETRY

(main steps, following the lectures of Iliopoulos [16(b)])

A.1 We start from the Lagrangian density

$$\mathcal{L}_1 = -\frac{1}{4}F_{\mu\nu}^2 + (D_\mu\phi)^2 - V(\phi)$$

$F_{\mu\nu} = \partial_\mu A_\nu - \partial_\nu A_\mu$ electromagnetic field; $D_\mu = \partial_\mu - ieA_\mu$ covariant derivative; $V(\phi) = M^2|\phi|^2 + \lambda|\phi|^4$ classical potential (complex)

$\mathcal{L}_1$ is invariant under gauge transformation $\phi \to e^{i\,(x)}\phi$, $A_\mu \to A_\mu + \partial_\mu\theta(x)$

(a) $M^2 \geqslant 0$

$\mathcal{L}_1$ describes QED for charged scalar particle.

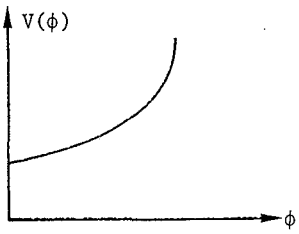

stable at $\phi = 0$

(b) $M^2 < 0$

perturbation theory around $\phi = 0$ yields unstable solution. Reach stable solution by transforming ϕ to $\phi' = 1/\sqrt{2}[a + \phi_1(x) + i\phi_2(x)]$.

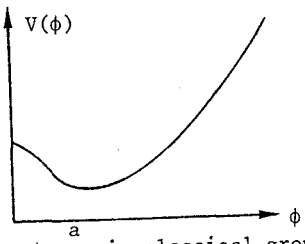

$\phi = a$ is classical ground state

A.2 $$\mathcal{L}_1 \to \mathcal{L}_2 = -\frac{1}{4}F_{\mu\nu}^2 + \frac{e^2a^2}{2}A_\mu^2 + \ldots + \frac{1}{2}[(\partial_\mu\phi_1)^2 - 2\lambda a^2\phi_1^2] + \frac{1}{2}(\partial_\mu\phi_2^2) - eaA_\mu\partial_\mu\phi_2 + \ldots$$

photon; massive vector; massive scalar; massless scalar

$\mathcal{L}_2$ is still gauge invariant (and is the form used to demonstrate renormalizability). The A_μ^2 term makes the gauge transformation more complicated

$\phi_1(x) \to [a + \phi_1(x)]\cos\theta(x) - \phi_2(x)\sin\theta(x) - a$, $\phi_2(x) \to [a + \phi_1(x)]\sin\theta(x) + \phi_2(x)\cos\theta(x)$,

$A_\mu \to A_\mu + \theta_\mu\theta(x)$

and implies a shift of the field.

In order to make the massless, unphysical field ϕ_2 (Goldstone boson) disappear, yet another transformation has to be chosen

$$\phi' = \frac{1}{\sqrt{2}}[a + \rho(x)]e^{i\chi(x)/a} \quad , \quad A_\mu(x) = B_\mu(x) + \frac{1}{a}\partial_\mu\chi(x)$$

A.3 $$\mathcal{L}_1 \to \mathcal{L}_3 = -\frac{1}{2}[B_{\mu\nu}^2 - e^2a^2B_\mu^2] + \frac{1}{2}[(\partial_\mu\rho^2 - 2\lambda a^2\rho^2] - \frac{\lambda}{4}\rho^4 + \frac{1}{2}e^2B_\mu^2(2a\rho + \rho^2)$$

massive vector B_μ; massive scalar ρ

$\mathcal{L}_3$ is no longer gauge invariant, but it contains only physical particles and their mass spectrum.

The original model of Weinberg (p 18) needs at least four vector bosons, W^+, W^- for ordinary weak interactions, Z^0 for the weak neutral currents and one (massless) for the photon (A_μ).

APPENDIX B

CHARMED PARTICLE STATES IN THE G.I.M. MODEL (from ref. [31])

TABLE I. Charmed $1/2^+$ baryon states.

	Label	Quark content	Isospin	Strangeness
$C=1$	C_1^{++}	cuu	$T=1,\ T_z=\begin{cases}1\\0\\-1\end{cases}$	$S=0$
	C_1^{+}	$c(ud)_{sym}$		
	C_1^{0}	cdd		
	C_0^{+}	$c(ud)_{anti}$	$T=0$	0
	S^{+}	$c(su)_{sym}$	$T=\frac{1}{2},\ T_z=\begin{cases}\frac{1}{2}\\-\frac{1}{2}\end{cases}$	-1
	S^{0}	$c(sd)_{sym}$		
	A^{+}	$c(su)_{anti}$	$T=\frac{1}{2},\ T_z=\begin{cases}\frac{1}{2}\\-\frac{1}{2}\end{cases}$	-1
	A^{0}	$c(sd)_{anti}$		
	T^{0}	css	$T=0$	-2
$C=2$	X_u^{++}	ccu	$T=\frac{1}{2},\ T_z=\begin{cases}\frac{1}{2}\\-\frac{1}{2}\end{cases}$	0
	X_d^{+}	ccd		
	X_s^{+}	ccs	$T=0$	-1

TABLE II. Charmed 0^- mesons.

	Label	Quark content	Isospin	Strangeness
$C=1$	D^{+}	$c\bar{d}$	$T=\frac{1}{2},\ T_z=\begin{cases}\frac{1}{2}\\-\frac{1}{2}\end{cases};$	$S=0$
	D^{0}	$c\bar{u}$		
	F^{+}	$c\bar{s}$	$T=0;$	$S=+1$
$C=0$	η	$\simeq (6)^{-1/2}(u\bar{u}+d\bar{d}-2s\bar{s}),$	$T=0;$	$S=0$
	η'	$\simeq \frac{1}{2}(u\bar{u}+d\bar{d}+s\bar{s}+c\bar{c}),$	$T=0;$	$S=0$
	η_c'	$\simeq (12)^{-1/2}(u\bar{u}+d\bar{d}+s\bar{s}-3c\bar{c})$	$T=0;$	$S=0$
$C=-1$	$\bar{D}^{0}$	$\bar{c}u$	$T=\frac{1}{2},\ T_z=\begin{cases}\frac{1}{2}\\-\frac{1}{2}\end{cases};$	$S=0$
	D^{-}	$\bar{c}d$		
	F^{-}	$\bar{c}s$	$T=0;$	$S=-1$

TABLE III. Charmed 1^- mesons.

$C=1$	D^{*+}
	D^{*0}
	F^{*+}
$C=0$	$\omega \simeq (2)^{-1/2}(u\bar{u}-d\bar{d})$
	$\phi \simeq s\bar{s}$
	$\phi_c \simeq c\bar{c}$
$C=-1$	$\bar{D}^{*0}$
	D^{*-}
	F^{*-}

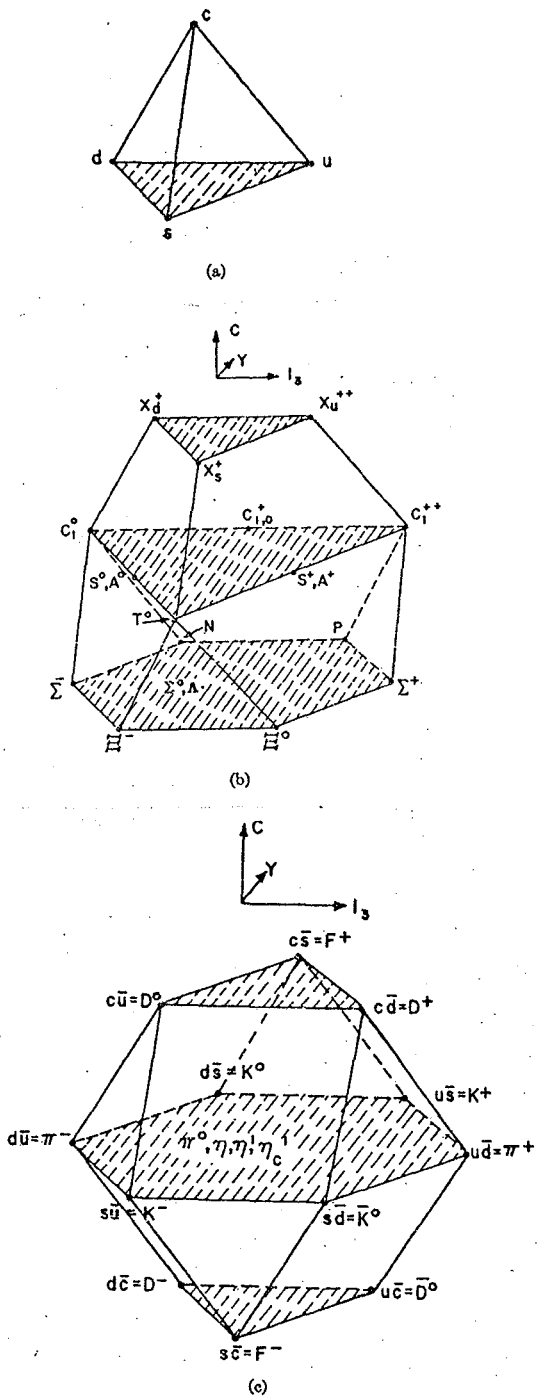

FIG. 1. Weight diagrams for SU(4). Shaded planes denote multiplets of SU(3) $\otimes$ U(1)$_C$. (a) The four quarks of SU(4): the conventional SU(3) triplet consisting of u ("up"), d ("down") and s ("strange") with $C=0$, and an SU(3) singlet c ("charmed") with $C=1$. (b) The three-quark $1/2^+$ baryons which form a 20-plet of SU(4). The SU(3) multiplets are 8 ($C=0$), 6 + 3 ($C=1$) and 3 ($C=2$). (c) The 15-plet + singlet pseudoscalars. The SU(3) multiplets are 3 ($C=-1$), 8 + 1 ($C=0$) and 3 ($C=+1$).

REFERENCES

[1] Suggestions for further reading:

(a) L.O. Okun, Weak Interaction of Elementary Particles, Pergamon Press (1965).

(b) C. Baltay, Interactions of Muon Neutrinos, in "Muon Physics", Eds V. Hughes and C.S. Wu, Academic Press 1975.

(c) Ch. Llewellyn-Smith, Physics Reports 3C (1972) 261.

(d) R. Marshak, Riazuddin and Ryan, Theory of Weak Interactions, Wiley 1969.

(e) C.S. Wu and S.A. Moszkowski, Beta Decay, Wiley 1966.

[2] W. Pauli, letter, 4 December 1930 (see ref. [1(e)] p. 385).

[3] E. Fermi, La Ricerca Scientifica 4 (1933) 491;
Zeits. für Physik, 88 (1934) 161.

[4] H.D. Dahmen, Herbstschule für Hochenergiephysik, Maria Laach, 1976.
C. Jarlskog, Proceedings of 1974 CERN School of Physics, CERN 74-22

[5] H.R. Crane and J. Halpern, Phys. Rev. 53 (1938) 1789.

[6] C.L. Cowan and F. Reines, Science 124 (1956) 103.

[7] G. Puppi, Nuovo Cimento 6 (1949) 194;
J. Tiomno and J.A. Wheeler, Rev. Mod. Physics 21 (1949) 153.

[8] R.P. Feynman and M. Gell-Mann, Phys. Review 109 (1958) 193.

[9] T.D. Lee and C.N. Yang, Phys. Review 104 (1956) 254.

[10] (a) C.S. Wu et al., Phys. Review 105 (1957) 1413.
(b) M. Goldhaber, L. Grodzins and A. Sunyar, Phys. Review 109 (1958) 1015.

[11] R. Marshak and E.C.G. Sudarshan, Phys. Review 109 (1958) 1860.

[12] J.J. Sakurai, Nuovo Cimento 7 (1958) 649.

[13] T.D. Lee and C.N. Yang, Phys. Review 119 (1960) 1410.

[14] Ch. Llewellyn-Smith, Proceedings IInd Tirrenia Study Week, CERN/ECFA/72-4, Vol. II (1973).

[15] G. Danby et al., Phys. Rev. Letters 9 (1962) 36.
Accurate confirmation by the CERN groups:
M. Block et al., Phys. Letters 12 (1964) 281;
J.K. Bienlein et al., Phys. Letters 13 (1964) 80.

REFERENCES (Cont'd)

[16] Ref. 1(d) , p. 225 and K. Borer et al., Proc. Vienna Conf. on Elementary Particles (1968).

[17] N. Cabibbo, Phys. Rev. Letters 10 (1963) 531.

[18] T. Eichten et al., Phys. Letters 40B (1972) 593.

[19] M. Gell-Mann, Phys. Letters 8 (1964) 214.
G. Zweig, CERN preprint 8182/Th 401 (1964).

[20] O.W. Greenberg, Phys. Rev. Letters 13 (1964) 598.
Also: S.L. Glashow, Quarks with Colour and Flavour, Sci. Am. 233, No. 4 (1975) 38.

[21] A. Bodek et al., Phys. Rev. Letters 30 (1973) 1087.
G. Miller et al., Phys. Review D5 (1972) 528.

[22] D.H. Perkins, Proc. of Topical Conference on Weak Interactions, CERN 69-7 (Yellow Report).

[23] F.J. Hasert et al., Phys. Letters 46B (1973) 121.
J. Blietschau et al., Nucl. Physics B114 (1976) 189.
For a spark chamber experiment, see H. Faissner et al., Proc. Int. Neutrino Conf. Aachen (1976) p. 221.

[24] F.J. Hasert et al., Phys. Letters 46B (1973) 138, Nucl. Physics B73 (1974) 1.

[25] A. Benvenuti et al., Phys. Rev. Letters 32 (1974) 800 and 1454.
B.C. Barish et al., Proc. XVIIth Intern. Conf. on High-Energy Physics (1974) paper No. 588.

[26] (a) Riazzuddin, Daresbury Lecture Note, No. 9 (1972).
(b) S. Weinberg, Rev. mod. Physics 46 (1974) 255.
(c) S. Weinberg, Scientif. American (1974).
(d) J. Iliopoulos, CERN 76-11 (Yellow Report).
(e) Ch. Llevellyn-Smith, Proc. Rutherford Lab. Meeting, February 1973.

[27] I. Bender, Herbstschule für Hochenergiephysik, Maria Laach (1975).

[28] S. Weinberg, Phys. Rev. Letters 19 (1967) 264.
A. Salam and J.C. Ward, Phys. Letters 13 (1964) 168.

REFERENCES (Cont'd)

[29] G. t'Hooft, Phys. Letters 37B (1971) 195.

[30] S.L. Glashow, J. Iliopoulos and L. Maiani, Phys. Review D2 (1970) 1285.

[31] M.K. Gaillard, B.W. Lee and J.L. Rosner, Rev. Mod. Physics 47 (1975) 277.

[32] T. Eichten et al., Nucl. Physics B44 (1972) 343

[33] S. Van der Meer, CERN/61-7 (Yellow Report).

[34] A. Asner and C. Iselin, CERN/65-17 and CERN/66-24 (Yellow Reports).

[35] H. Wachsmuth, Symposium on Beam Intensity Measurement, DNPL/R1 (1968) 68, and CERN Neutrino Meeting, CERN/69-28 (Yellow Report) 33.

[36] W. Venus and H. Wachsmuth, CERN/TC-L/Int. 75-3 (1975).

[37] C. Henderson, Cloud and Bubble Chambers, Methuen and Co., London 1970;
Yu. A. Aleksandrov et al., Bubble Chambers, Indiana Univ. Press 1967.

[38] B. Roe et al., NAL-Summer Study 1969.

[39] R.P. Shutt (ed.), Bubble and Spark Chambers, Acad. Press, NY London 1967

[40] W.H. Barkas, Nuclear Research Emulsions, Acad. Press, NY London (1963) Vol. I and (1973) Vol. II.

[41] I. Budagov et al., Lettere al Nuovo Cimento (I) 2 (1969) 689.

[42] M. Holder et al., Nuovo Cimento 57 (1968) 338;
R.L. Kustom et al., Phys. Rev. Letters 22 (1969) 1014.

[43] S.J. Barish et al., Int. Symp. on Lepton and Photon Interactions, Stanford (1975) and ANL-HEP-PR-76-66;
W.A. Mann et al., Phys. Rev. Letters 31 (1973) 844.

[44] (a) A. Pais, Annals of Physics 63 (1971) 361.
(b) (cf. ref. 1(b)); Calculation shown in detail by M. Block, in International School of Physics "Ettore Majorana" (1964) 341.

[45] I. Budagov et al., Phys. Letters 29B (1969) 524.
J. Campbell et al., Phys. Rev. Letters 30 (1973) 335.
P. Schreiner and F.V. Hippel, Phys. Rev. Letters 30 (1973).

REFERENCES (Cont'd)

[46] N. Cabibbo and F. Chilton, Phys. Review 137B (1965) 1628.

[47] T. Eichten et al., Phys. Letters 46B (1973) 274.

[48] S.J. Barish et al., Colloque International du CNRS, Physique des Neutrinos à Haute Energie, Paris (1975) and

Argonne Nat. Lab. Preprints ANL-HEP-CP-75-40, ANL-HEP-75-38 and COO-1428-424.

[49] A. Benvenuti et al., Phys. Rev. Letters 32 (1974) 125.

[50] B.C. Barish et al., Phys. Rev. Letters 35 (1975) 1316.

[51] M. Gourdin, CERN School of Physics 1972, CERN/72-17 (Yellow Report).

[52] Note added in proofs:
First Analysis of CERN ν-experiments with the SPS narrow-band beam and recent analysis of the CAL-TEC-FNAL experiment show less increase of $\sigma^{\bar{\nu}}/\sigma^{\nu}$ and no high y anomaly.

[53] T. Eichten et al., Phys. Letters 46B (1973) 281.
A paper on analysis using more statistics is in preparation.

[54] B.W. Lee, Proceedings of Neutrino 1976 Conference, Aachen (1976).

[55] A. Benvenuti et al., Phys. Rev. Letters 34 (1975) 419 and Phys. Rev. Letters 35 (1975) 1199, 1203 and 1249.

[56] B. Barish et al., Symposium on Lepton and Photon Interactions, Stanford (1975).

[57] A. Pais and S. Treiman, Phys. Rev. Letters 35 (1975) 1205.

[58] (a) U. Nguyen-Khac, Colloque International du CNRS, Physique du Neutrino à Haute Energie, Paris (1975) 173.

(b) J. Blietschau et al., Phys. Letters 60B (1976) 207.

[59] J. von Krogh et al., Phys. Rev. Letters 36 (1976) 710 and 38 (1977) 1248.

C. Baltay et al., Proc. Am. Phys. Soc. Meeting, Division of Particules and Fields (1976).

[60] D.H. Perkins, P. Schreiner and W.G. Scott, CERN/EP/PHYS 77-4, preprint submitted to Phys. Letters B.